REPORT DOCUMENTATION PAGE

Form Approved OMB No. 0704-0188

1. REPORT DATE *(DD-MM-YYYY)*	2. REPORT TYPE	3. DATES COVERED *(From – To)*
26-07-2010	Final Report	23 July 2009 - 23-Jul-10

4. TITLE AND SUBTITLE

Centrifugal Spray Generator of Singlet Oxygen for a COIL

5a. CONTRACT NUMBER
FA8655-09-1-3091

5b. GRANT NUMBER

5c. PROGRAM ELEMENT NUMBER

6. AUTHOR(S)

Dr. Jarmila Kodymová

5d. PROJECT NUMBER

5d. TASK NUMBER

5e. WORK UNIT NUMBER

7. PERFORMING ORGANIZATION NAME(S) AND ADDRESS(ES)

Institute of Physics, Academy of Sciences CR
Na Slovance 2
Prague 8 182 21
Czech Republic

8. PERFORMING ORGANIZATION REPORT NUMBER

N/A

9. SPONSORING/MONITORING AGENCY NAME(S) AND ADDRESS(ES)

EOARD
Unit 4515 BOX 14
APO AE 09421

10. SPONSOR/MONITOR'S ACRONYM(S)

11. SPONSOR/MONITOR'S REPORT NUMBER(S)
Grant 09-3091

12. DISTRIBUTION/AVAILABILITY STATEMENT

Approved for public release; distribution is unlimited.

13. SUPPLEMENTARY NOTES

14. ABSTRACT

This report results from a contract tasking Institute of Physics, Academy of Sciences CR as follows: B.Technical Proposal / Description of Work:
The research on development the CentSpraySOG could not be accomplished within the previous contract duration, and therefore we would like to solve the remaining problems in order to improve still the device parameters in framework of this new contract. The work on the tasks can be described briefly as follows:
To optimize the generator efficiency: to improve the Cl2 utilization at simultaneously high
O2(1delta) yield. This would be attained e.g.
(i) by a constructional modification of the CentSpraySOG device, enabling to vary reaction volume and so the gas residual time in the reaction space and separator at a high input Cl2 pressure, (ii) by using a more concentrated BHP,
(iii) by optimizing a Cl2/He ratio at the generator input,
(iv) by decreasing a diameter of the BHP droplets.

15. SUBJECT TERMS
EOARD, Laser physics, Laser engineering

16. SECURITY CLASSIFICATION OF:			17. LIMITATION OF ABSTRACT	18, NUMBER OF PAGES	19a. NAME OF RESPONSIBLE PERSON
a. REPORT	b. ABSTRACT	c. THIS PAGE			A. GAVRIELIDES
UNCLAS	UNCLAS	UNCLAS	UL	43	19b. TELEPHONE NUMBER *(Include area code)* +44 (0)1895 616205

DEPARTMENT OF THE AIR FORCE
HEADQUARTES, 603D REGIONAL SUPPORT GROUP (USAFE)
European Office of Aerospace Research and Development (EOARD)
86 Blenheim Crescent, Ruislip, Middlesex HA4 7HB, UK

Final Report

Referring to

Grant No.FA8655-09-1-3091

Effective date 23 July 2009

Title	**Centrifugal Spray Generator of Singlet Oxygen for a COIL**
Principal Investigator	Jarmila Kodymová
Co-Investigators	Otomar Špalek, Vít Jirásek, Miroslav Čenský Department of Chemical Lasers Institute of Physics AS CR
Technical Advisor	Dr. Timothy Madden High Power Gas Lasers Branch US AF Research Laboratory Directed Energy Directorate Kirtland AFB, NM, USA
Grant Awarded to	Institute of Physics, Academy of Sciences CR Na Slovance 2 182 21 Prague 8 Czech Republic Phone: +420 266 052 699 Fax: +420 286 890 265 E-mail: kodym@fzu.cz
Date of Submission	22 July 2010 12 months after start of period of performance

Contents

1. General information about the grant

1.1. Outline of the project subject

The grant was awarded to design, develop and parametrically study a new type of the generator of singlet oxygen for a COIL, a Centrifugal Spray Singlet Oxygen Generator (abr. CentSpraySOG). The CentSpraySOG operates with a gas-liquid reaction based on the conventional chlorine-basic hydrogen peroxide chemistry like e.g. a jet SOG employed in the COIL technology so far. The new SOG concept should take advantage of the Cl_2/BHP spray system providing a large interface area for a singlet oxygen generation, and of efficient separating the generated singlet oxygen, $O_2(^1\Delta)$, from the liquid by means of the centrifugal force effect. A detailed theoretical study of the CentSpraySOG operation parameters performed in the previous grant project, FA8655-05-C-4022 *Advanced singlet oxygen generator for a COIL* [1], predicted generation of a high $O_2(^1\Delta)$ yield (up to 80%) at even a high total pressure in the generator (up to 75 kPa, i.e. 560 Torr), and a high chlorine utilization (up to 95%). The generator can operate independently on gravitation and its frame acceleration, which could be beneficial for driving the COIL employed in a mobile (airborne) application. The modeling results were a good base for designing the small-scale device to test the CentSpraySOG operation parameters experimentally.

The experimental results on the CentSpraySOG presented in the Final EOARD Report of the previous grant project ended in April 2008 [2], and also in Refs. [4-7] can be summarized as follows: A rather high product $U_{Cl}Y_{\Delta}$ (Cl_2 utilization and $O_2(^1\Delta)$ yield) in the range of 0.6–0.8 was attained at the generator pressure of 20–30 kPa (150–225 Torr), or 0.4–0.6 at 40–60 kPa (300– 450 Torr), respectively. The $O_2(^1\Delta)$ partial pressure increased up to 4 kPa (30 Torr) at the generator pressure of 60–70 kPa (450–525 Torr). By termination of the Report [2], a direct measurement the Cl_2 utilization and the $O_2(^1\Delta)$ yield started. First results of the $O_2(^1\Delta)$ yield ranged from 0. 3 to 0.75, the Cl_2 utilization from 0.64 to 0.84 for the$O_2(^1\Delta)$ partial pressure from 2.2 to 4 kPa (16.5–30 Torr) and the generator pressure ranging from 30 kPa to 70 kPa (225–525 Torr). The BHP utilization was also very high (20–80%). The separation of liquid from gas exiting the generator was investigated first in "model" conditions, i.e. using NaOH as liquid and N_2 gas, and then with the Cl_2/BHP exothermic reaction system. An initial rotation speed 4,000 r.p.m. of the generator centrifugal separator was insufficient to get a satisfactory separation, so that the separator was then operated with a speed from 7,000 to 9,000 r.p.m. A comparing the CentSpraySOG parameters with relevant parameters published on the rotating disc and jet singlet oxygen generators showed that similar values of the $O_2(^1\Delta)$ yield and Cl_2 utilization were measured with the CentSpraySOG at much higher generator pressure and with much better BHP utilization. This could be beneficial for a high pressure COIL operation and reducing a weight of the COIL device thanks to a less amount of BHP consumption for adequate $O_2(^1\Delta)$ production.

1.2. Tasks and supplies in the grant proposal

A) Optimization of the generator efficiency expressed as a product $U_{Cl}Y_{\Delta}$ (U_{Cl} is the Cl_2 utilization, Y_{Δ} is the $O_2(^1\Delta)$ yield). This will be attained by
   a) constructional modifications of the device resulting in reduction of the residence time of $O_2(^1\Delta)$ in the separator space,
   b) more precise determination of the residual Cl_2 in gas exiting the generator,
   c) increased $[HO]_2^-$ using more concentrated BHP,
   d) increased ratio of Cl_2 to He flow rate into the generator.

Detailed results were given in the Report 001 of this grant.

B) In accord with the modeling results of the separator to improve the centrifugal separator efficiency regarding to droplets of the diameter > 0.5 μm, achievable by
   a) constructional modifications of the separator rotor,
   b) designing a new separator with more than two slits in the rotor walls.

   The Spraytec Malvern instrument will be used for in situ study of the droplet content in the gas exiting the CentSpraySOG separator.

Results were partly given in the Report 001 of this grant except for the task ad b).

C) On-line data acquisition of most parameters (flow rates of all gases, temperature and pressure at all important points of the device, rotation speed of the separator, diagnostics, etc.).

The task was fulfilled partly during a research period of the Report 001 and partly during a period of the Report 002 of this grant.

D) Constructional modifications of the CentSpraySOG device and laser body to prepare a testing of the COIL (4-cm-gain length) driven by the CentSpraySOG; measuring the laser gain and power in dependence on the SOG parameters.

Solving the task started during the research period of the Report 002, and continued during this last period of this grant.

E) Calculations and modeling of processes in the COIL driven by the CentSpraySOG, supporting the constructional modifications of the device and interpretation of experimental results.

The task was solved continuously during the grant duration.

D) In addition to the tasks defined in the grant proposal, a new chemical method of molecular iodine generation was developed and successfully tested on the supersonic COIL.

Results were given partly in the Report 001, partly in the Report 002 and summarized with additional results in this Final report.

2. Principle of the CentSpraySOG device operation

The centrifugal spray SOG is schematically shown in **Fig. 1a,** and a gas-liquid (two-phase) nozzle for a spray formation from introduced chlorine-BHP reagents is shown in **Fig. 1b**.

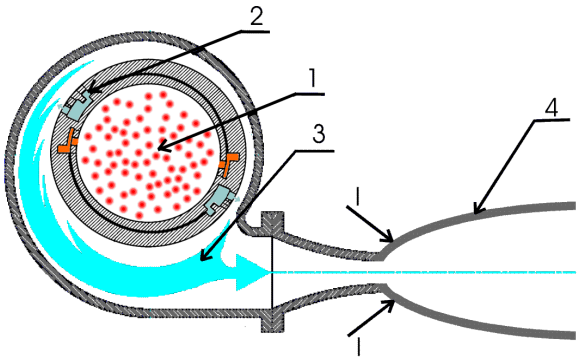

Fig.1a. Scheme of CentSpraySOG coupled to laser nozzle
1-spray of BHP-Cl_2/He mixture, 2-rotating separator,
3- gas stream with $O_2(^1\Delta_g)$, 4-laser nozzle, I-iodine injection

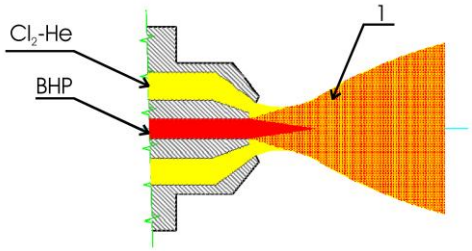

Fig.1b. Scheme of two-phase spray nozzle
1-spray of BHP-Cl_2/He mixture

The atomizing nozzle is a crucial component of the generator. It should form the fine BHP spray containing droplets of uniform size (~20 μm) from very viscose BHP liquid (5–35 mPas). Fig. 1b shows the nozzle with external gas and liquid mixing with controlling independently their flow rates, used in the designed CentSpraySOG. Depleted BHP liquid is separated in the rotating cylindrical separator by inertial and centrifugal forces. In **Figs. 2a** and **2b**, a technical drawing of the separator cross-section and a 3-D view of the separator are shown.

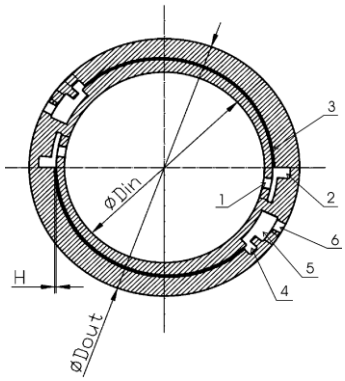

b)

a)

Fig. 2. Cross-section and 3-D view of the centrifugal separator. Reactor diameter D_{in}= 37 mm, separator outer diameter D_{out} = 50 mm, reactor length a = 50 mm, 29 impactor holes of diameter d_i = 3 mm (in each channel), slit height H = 0.8 mm, slit length L_{slit}= 43 mm.

The principle of the separation process is following. Most of BHP droplets of the spray are separated by impact on inner cavity wall of the separator rotor after acceleration during the passage through the holes 1 drilled in the wall. A captured liquid is drained through two channels 2 parallel with the axis of rotation. Finer droplets remaining in the gas are afterwards separated in two annular slit channels 3 by settling on the slit wall by a high centrifugal acceleration (350-2200 *g* at 4,000-10,000 r.p.m.). A liquid separated in these slits is drained through channels 4 and exits the separator drum through channels in the separator base. A gas containing $O_2(^1\Delta_g)$ exits the separator through channels 5 and two rows of exit holes 6.

3. Experimental devices and measuring techniques in use

3.1. The CentSpraySOG hardware

The CentSpraySOG prototype device was constructed following-up the modeling results and experimental results obtained on auxiliary devices afore described in Reports of the previous grant [1,2]. Hardware of the device is shown on the photo in **Fig. 3**, and the rotor shell with two slits and distributing rotor flange is shown on the photo in **Fig. 4.**

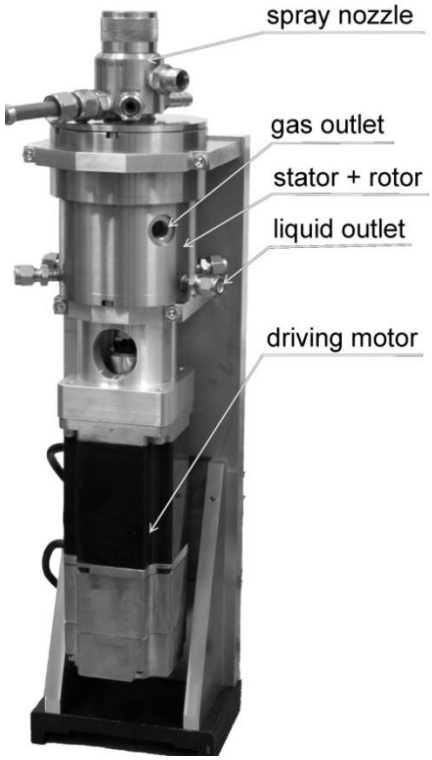

Fig. 3. Hardware of the CentSpraySOG

Fig. 4. Photo of rotating separator with slits and distributing rotor flange

An inner volume of the rotating separator with cylindrical reaction cavity is 68.7 cm^3. The separator rotor was made either of stainless steel or titanium to compare the $O_2(^1\Delta)$ quenching on both metal surfaces. Fabrication of the slits, collecting channels (items 2, 4, 5 in Fig. 2a), and two rows of 3 mm-holes in the separator wall for the spray entrance (29 holes at each channel input) were made by a computer controlled electro-erosive machining. Nine 3 mm-holes 6 were drilled in one row for each slit for the gas outlet from the separator rotor.

The separator rotor was substantially improved during this research period because a friction in the former large rotor bearing caused a great heating of the separator together with large sealing. The former rotor with large bearing and distributing flange was replaced with a newly fabricated rotor fixed from one side only, and was equipped with one small bearing only. This new rotor was shown in Fig. 3 of the interim Report [20]. This modification reduced the friction heating in the separator and improved a tightness of the generator space.

Three types of separator driving motors were subsequently employed. A powerful motor (type ABB Servomotor SDM631-012N0-140 with a frequency converter ACS550) providing a rotation speed up to 10,000 r.p.m. was finally employed.

3.2. Experimental set up for study of the CentSpraySOG parameters

Parametric study of the CentSpraySOG itself was performed on the experimental set-up shown on the photo in **Fig. 5**, and details with detection cells for $O_2(^1\Delta)$ and Cl_2 monitoring at the generator exit on the photo in **Fig. 6.**

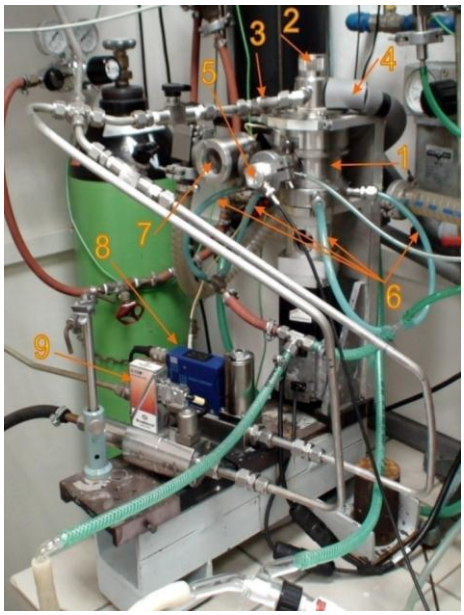

Fig. 5. Photo of set-up with the CentSpraySOG

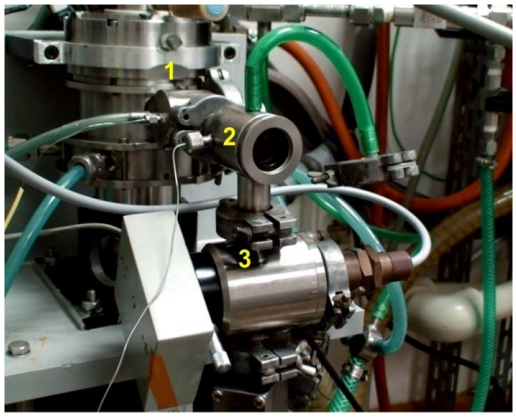

Fig. 6. Photo of detail with detection cells
1 – CentSpraySOG, 2 – optical cell for $O_2(^1\Delta)$ detection,
3 – optical cell for Cl_2 detection

The spray nozzle 2 (type SAM-06-04 BETE Comp., USA) was fixed on the top of generator-reactor body 1. The BHP liquid prepared by mixing of 50% H_2O_2, 50% KOH, and water (resulting HO_2^- concentration 5.3 M or 7.5 M) was introduced into the spray nozzle from a cooled tank (not shown) by pressurized N_2. Chlorine was introduced into the nozzle from a 40-liter pressurized gas cylinder through a pressure reducer and mass flow regulator 8 (M+W Instruments GmbH, Germany, type D-6251/8mm-SS). A parallel gas line with pressure reducer and mass flow regulator 9 (Bronkhorst, Netherlands, type F-202AC-FBB-44-V) served for the helium introducing. Helium and chlorine were mixed before the nozzle inlet (the line 3).

The gas exited the generator through the centrifugal separator was flowing through the optical cell for $O_2(^1\Delta)$ detection (5 in Fig. 5 and 2 in Fig. 6), and the optical cell for residual chlorine detection (7 in Fig. 5 and 3 in Fig. 6). The gas was then exhausted by a rotary pump (150 m^3/h). The liquid exiting the centrifugal separator was leaving the device through four tubes 6 and was collected in a bottle underneath. The pressure of gas and liquid upstream the nozzle and in the reactor was measured by pressure gauges and manometers.

The $O_2(^1\Delta)$ emission at 1270 nm in the inner space of detection cell was monitored by the Ge photodiode with active diameter of 5 mm (Judson Technologies, LLC, PA, USA, type J16- 5SP-R05M-SC). Photodiode responsivity was 0.6 A/W, and the gain of commercial preamplifier (type PA-7-70, Judson Technologies, LLC, PA, USA) was $1x10^7$ V/A. An interference filter (CVI Laser LLC) with 53.2% transmission at 1.27 μm was used to filter the emitted light. A calibration constant, k_Δ, determining a relation between the $O_2(^1\Delta)$ partial pressure and output voltage of photodiode current amplifier was calculated for given optical cell geometry, filter transmission, and diode responsivity. The constant k_Δ = 976.2 Pa/V at 315 K was used. The $O_2(^1\Delta_g)$ yield, Y_Δ, was calculated by the relation

$$Y_\Delta = p_\Delta \, n_{tot} / (n_{Cl2} \, U_C \, p) \qquad (1)$$

where p_Δ is the measured $O_2(^1\Delta_g)$ partial pressure, n_{tot} is the total molar gas flow rate, n_{Cl2} is the Cl_2 molar flow rate, U_C is the Cl_2 utilization, and p is the pressure in the $O_2(^1\Delta_g)$ detection cell.

Chlorine utilization, U_C, was calculated from the equation

$$U_C = 1 - \frac{c_{C(res)}}{c_{C(in)}} \qquad (2)$$

where $c_{C(res)}$ is the concentration of residual chlorine, and $c_{C(in)}$ is the chlorine concentration at the generator input. The concentration of residual chlorine was calculated from the light absorption at a wavelength of 350 nm measured by the spectral photometer Spektrum 10 (Unilab, CR) using the

absorption cross section of 18.8 x 10^{-20} cm^2. The input Cl_2 concentration was calculated by the formula

$$c_{C(in)} = \frac{n_{Cl2}}{n_{Cl2} + n_{He}} \frac{p_{gen} N_A}{RT} \qquad (3)$$

where n_i is the molar flow rate of species i at the generator input, p_{gen} is the generator pressure, R is the gas constant, and N_A is the Avogadro constant.
The BHP utilization, U_{BHP}, was calculated as

$$U_{BHP} = 2\, U_C\, n_{Cl2}/(v_{BHP}\, c_H) \qquad (4)$$

where v_{BHP} is the BHP flow rate, and c_H is the HO_2^- concentration in the input BHP solution.

Separation efficiency of the CentSpraySOG was studied in several experimental series by means of the instrument SPRAYTEC, Malvern Instruments, lent by the Institute of Thermomechanics AS. In the first few tests, water and nitrogen were used in the generator operation, and the exiting gas was directed into the space between two Spraytec heads, one serving as a laser light emitter, the second as a light detector. The laser beam passed perpendicularly to the gas stream. In further experiments performed with the BHP/Cl_2 reaction spray, an optical diagnostic cell was attached to the CentSpraySOG exit. The cell of inner length 10 cm was equipped with two windows, the output one with an antireflective coating on both sides. The laser beam passed via these windows through the cell, parallel to the gas flow. This arrangement is shown in **Fig. 7**.

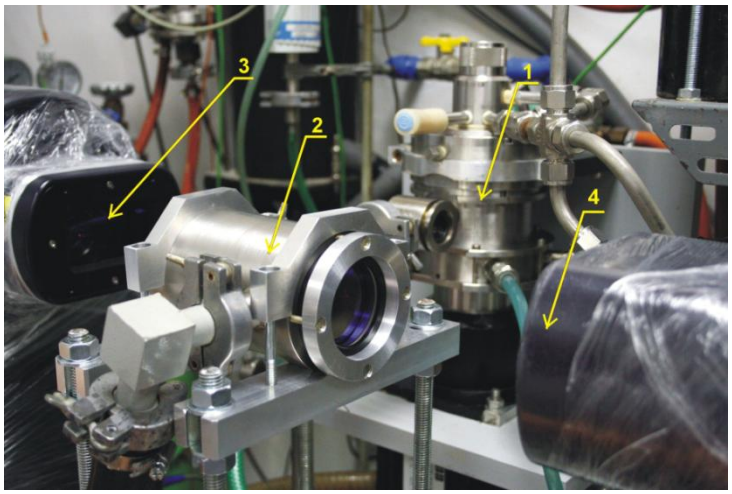

Fig. 7. Experimental arrangement for studies of the separation efficiency
1 – CentSpraySOG, 2 – optical cell for analyzing droplets in gas flowing from the generator,
3 – Spraytec head with the laser beam source, 4 – Spraytec head with detector

3.3. Experimental set up of supersonic COIL driven by the CentSpraySOG

A photo of the experimental device is shown in **Fig. 8**. The BHP liquid is prepared by mixing 1.0 litre of H_2O_2 (50% b.w.) and 1.5 litre of KOH (50% b.w.) in mixing tank *1*. Liquid is transferred after cooling down to about -28°C into the BHP input tank *2* through isolated stainless steel piping. Pressure in this tank is increased to 180-220 kPa (abs.) by means of pressurized nitrogen just before the generator operation. The BHP liquid is then led by isolated stainless steel tubes through the flow meter into the atomizing spray nozzle of the SOG *3*. Primary gas mixture of Cl_2 and He for the singlet oxygen generation is prepared in the same way as described in the chapter 3.2., and is introduced by a stainless-steel pipe into the spray nozzle fixed in the generator top *4.* A rotation speed of the separator rotor is controlled by PC on line. The gas pressure in the generator is adjusted by a removable choking nozzle with suitably selected cross-section. This nozzle is inserted into the outlet of the generator of 16 mm i.d. Several nozzles were fabricated and tested with a different number of openings. Each opening itself is machined as a miniature converging-diverging nozzle to minimize the friction losses and gas whirling. The gas with generated $O_2(^1\Delta)$ then flows through the input "delta" channel *6* of the laser body, where the channel cross-section is expanded to a width of 40 mm and a height of 10 mm. The supersonic nozzle *7* in combination with the iodine injector is described in chap. 3.3. The supersonic nozzle further continues into the laser body *8* equipped with two arms connecting the N_2 purge segments *9* and optical wedges *10*. The gas further passes through the duct elbow *11* and the delta channel *12* into the LN_2 trap *13* with copper ribs. The gas is then exhausted through the vacuum piping into by the pumping complex with a pumping capacity of 1500 m^3/h or 3600 m^3/h, depending on the total gas flow rate.

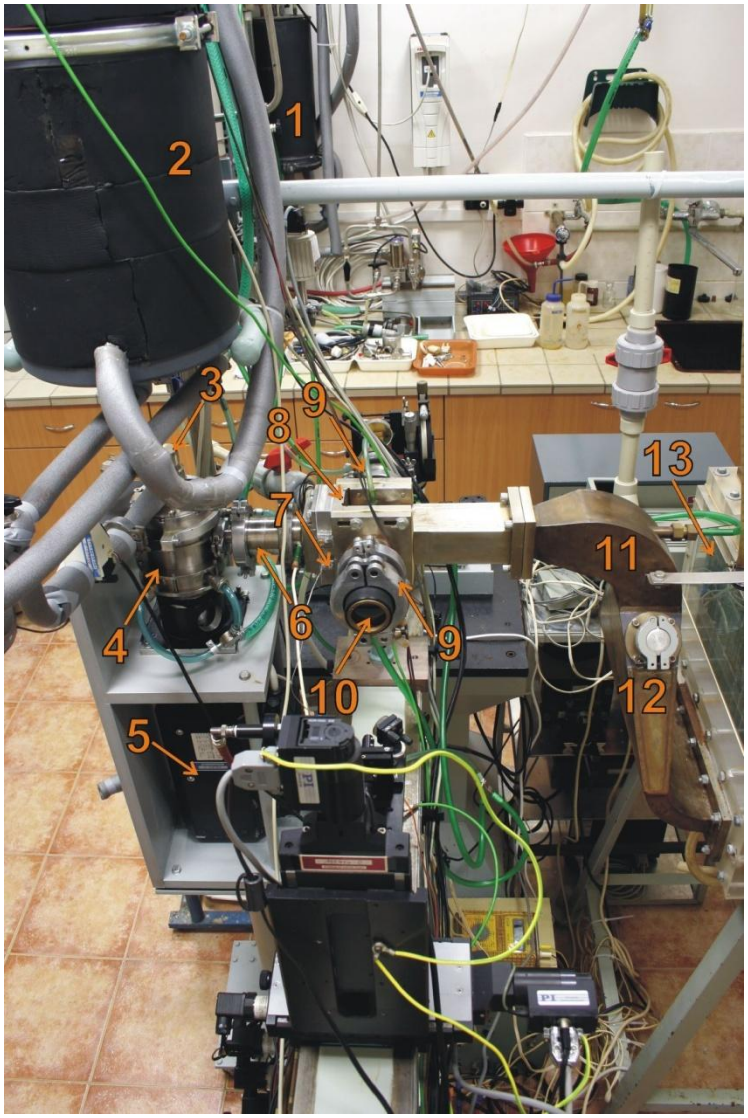

Fig. 8. Overall view on the laser from the right side
1 – BHP mixing tank, *2* – pressurized BHP tank, *3* – atomizing nozzle, *4* – centrifugal spray generator, *5* – driving motor, *6* – input delta channel, *7* – I_2 injector with supersonic nozzle throat, *8* – nozzle body, *9* – N_2 purge, *10* – optical wedges, *11* - duct elbow, *12* – delta channel, *13* – water and iodine trap

Other parts of the apparatus from the opposite view are visible in **Fig. 9.** In this photo you can see, except parts described in Fig. 7, the BHP outlet from the generator. The BHP liquid flows from the separator through 4 tubes *10* into the collecting bottle *11* made of industrial glass. The spectral photometer *12* for measuring a residual chlorine concentration, the Ar ion laser *13* and Si photodiode amplifier *14* for detection of I_2 concentration are placed on the stand visible on the left side.

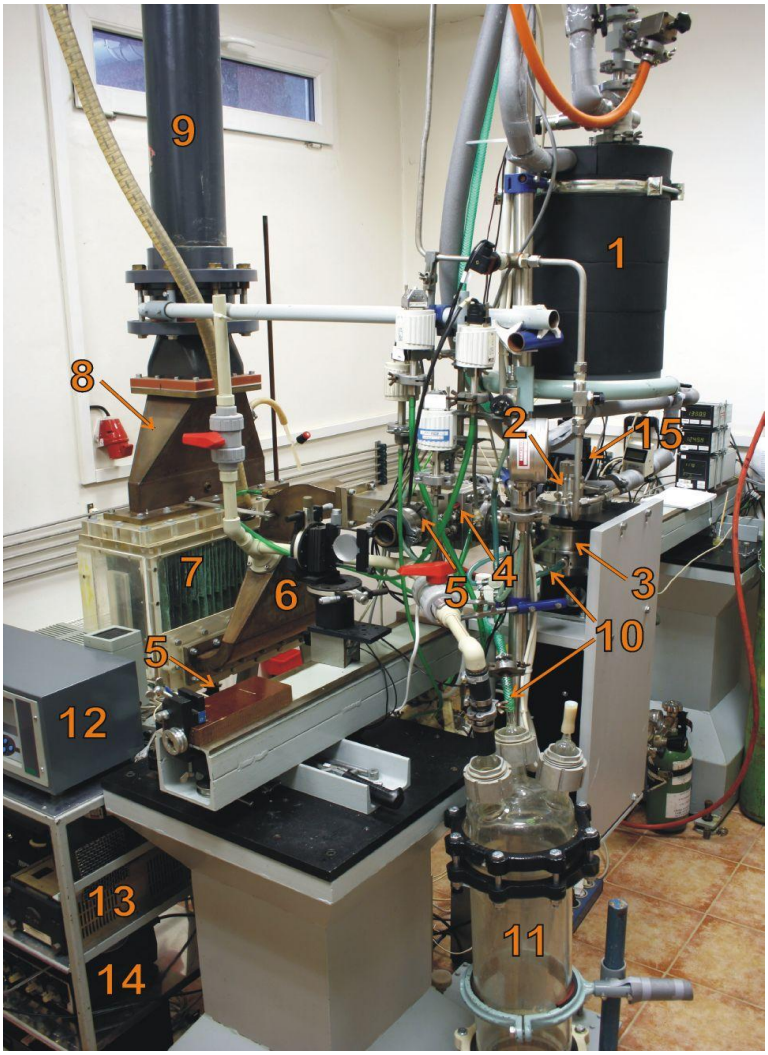

Fig. 9. Overall view on the laser from the left side
1 – pressurized BHP tank, *2* – atomizing nozzle, *3* – centrifugal spray generator, *4* – I_2 injector with supersonic nozzle throat, *5* – nozzle body purge and optical wedges, *6* – input delta part of the trap, *7* – water and iodine trap, *8* – exit delta chanell, *9* – vacuum piping, *10* – outlet BHP tubes, *11* – outlet BHP bottle, *12* – spectral analyzer for residual Cl_2, *13* – Ar ion laser for I_2 detection, *14* – amplifier for I_2 detection signal, *15* – diode probe laser emitter/detector on positioning unit

A detailed view on the generator attached to the laser body is in **Fig. 10**. The atomizing nozzle *1* is on the top of the generator *2*. The BHP liquid is inlet from the pressurized tank through the isolated tube *3* and the flow meter *4*. The separator is fixed to the stand *5* by the flange *6*. Two of four tubes *7* for the BHP outlet are visible in this figure. The emitter and detector of the diode probe laser *8* for diagnostics

of atomic iodine in the resonator region is on the left side of this figure. One optical wedge mount *9* and the nozzle body *10* are also shown here.

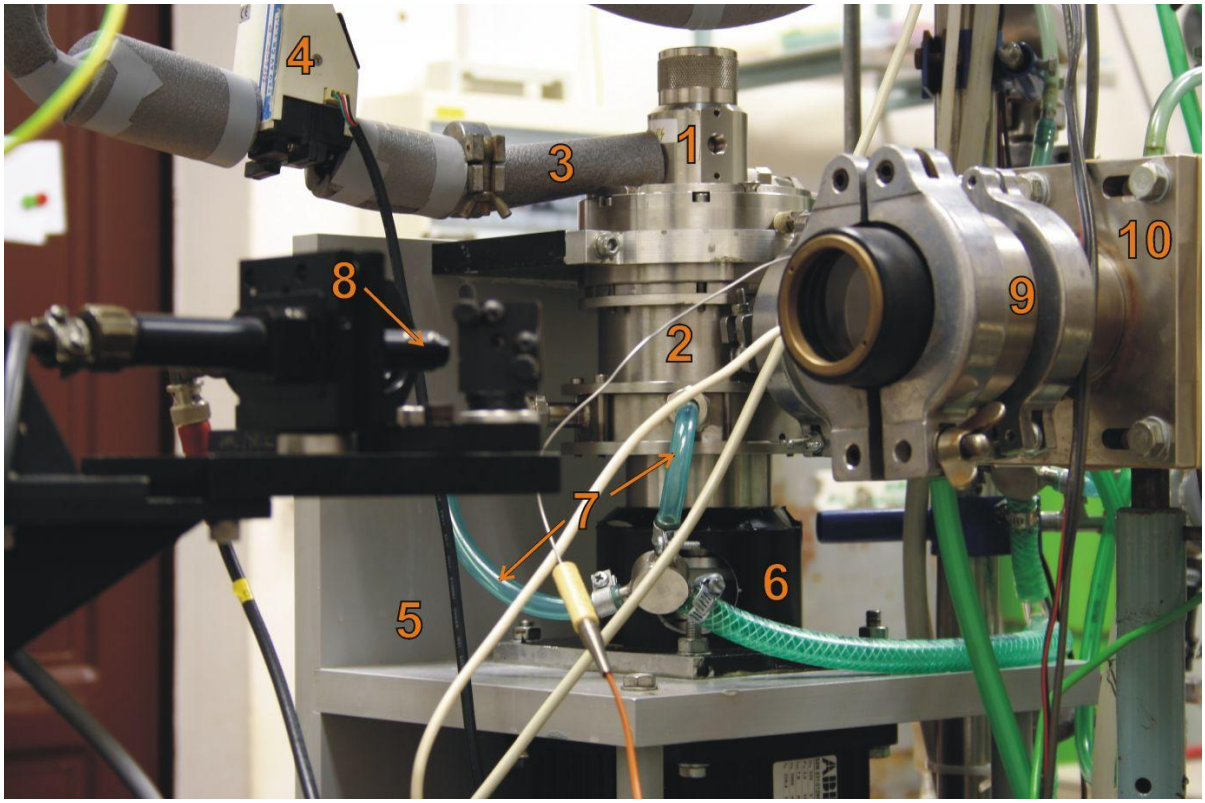

Fig. 10. Detailed view on the centrifugal spray generator
1 – atomizing nozzle, *2* – centrifugal spray generator, *3* – input BHP tube, *4* – BHP flow meter, *5* – stand, *6* – generator fixing flange, *7* – BHP outlet tubes, *8* – diode probe laser emitter/detector on positioning unit, *9* – optical wedge mount, *10* – nozzle body

Two arrangements of iodine injection were used - supersonic or subsonic. A cross-section of the supersonic iodine injector is shown in **Fig. 11a**. A cross-section of entrance of the primary gas channel was 6.6 x 40 mm; the channel was then narrowed to a critical section of 3.7 x 40 mm, and then expanded to 6.4 x 40 mm. In laser body, the bottom and upper walls of the channel farther form the angle 2° related to the cavity axis. Secondary nitrogen or helium containing iodine vapor was introduced into the holes H and was injected into the primary flow through one row of 16 conical holes, *H*, of diameters 1.4/1.9 mm. The centres of the injector holes were located 2.8 mm downstream of the critical section of the nozzle. The bottom and upper rows of openings were arranged in a staggered configuration. The injector was electrically heated by means of two cartridge heaters to 65-80°C. A cross-section of the subsonic injector is shown in **Fig. 11b.** Iodine is injected through one row with 16

holes of diameter 0.55 mm, *H1*, located 8 mm upstream of the critical section of the nozzle and one row of 15 holes (H2) of diameter 0.35 mm located 6 mm upstream of the critical section. The shape of the primary gas channel and the heating are the same as for the supersonic injector.

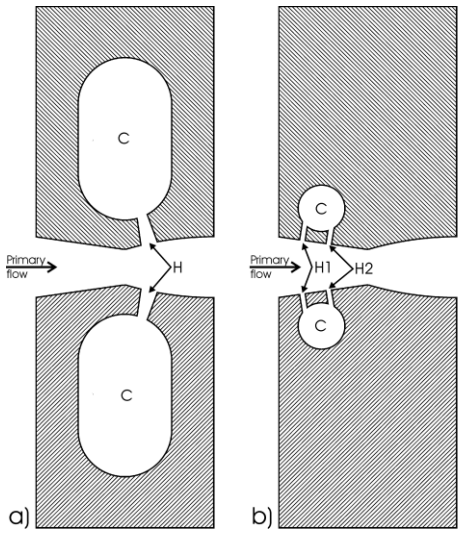

Fig. 11. Cross sections of supersonic **(a)** and subsonic injector **(b)**

The iodine vapor was generated either by the all-gas chemical method described in the chapter 5 or by evaporation of solid iodine, when a bed of iodine crystals was placed in a stainless-steel tube of inner diameter 4 cm (volume of 0.38 litre). The evaporator was heated by hot air fan and the continuing pipe was wrapped by heating bands maintained at the temperature of 70-90°C. Nitrogen or helium used as a carrier of I_2 vapour passed through this bed, and entered the optical cell for detection of I_2 concentration by Ar^+ laser at 503 nm (the same as in chapter 5). The mixture was then introduced through two heated Teflon tubes into the iodine injector *7*. The injector was electrically heated by means of two cartridge heaters to the temperature of 65-80°C.

A detailed view on the generator and iodine injector is shown in **Fig. 12.** The gas exiting the generator *1* flows through the exchangeable pressure reducing nozzle, input delta channel *2* and adaptive flange *3* into the iodine injector *4*. Subsonic channel is in the input delta channel *2* and the adaptive flange *3*, the throat in created in the I_2 injector. The input delta channel, the adaptive flange *3*, and the I_2 injector are connected with the nozzle body *5* by means of four M8 screws.

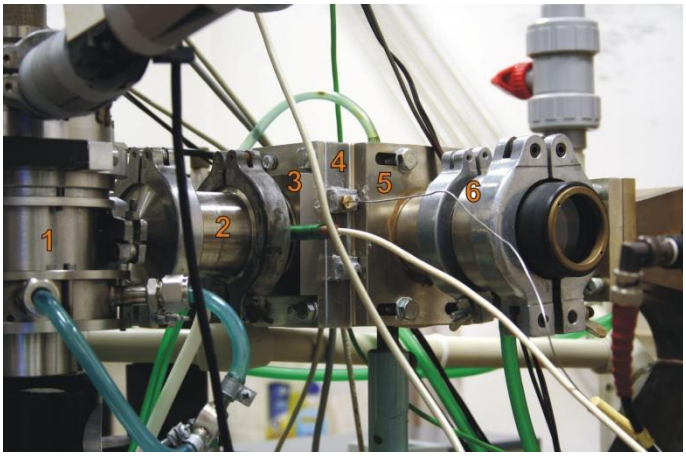

Fig. 12. Detailed view on the generator and I_2 injector
1 – centrifugal spray generator, *2* – input delta channel, *3* – adaptive flange, *4* – I_2 injector, *5* – nozzle body, *6* – holder of optical window.

The chemical I_2 reactor is shown in **Fig. 13**. Reactive gases, i.e. $Cl_{2,sec}$ and HI, and $N_{2,sec}$ are mixed in two common T-pieces. This mixture enters the reactor *4* made of stainless steel tube of inner diameter 4 cm and total length of 90 cm, heated with heating bands to ~ 90 °C. The gas mixture with formed I_2 enters the diagnostic cell *5*, where the I_2 concentration is monitored from the absorption of 503 nm-light emitted by the Ar^+ laser. The light after passing the cell is detected by the Si photodiode. The reactor pressure is maintained between 8 kPa and 12 kPa and is controlled by the valve *8* at the cell exit.

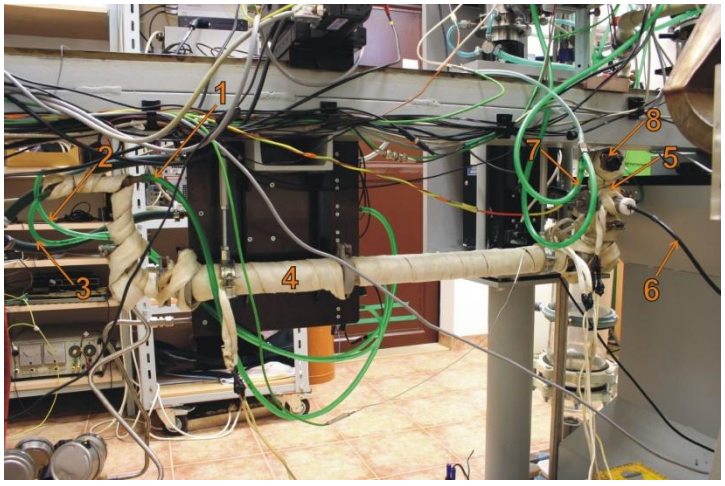

Fig. 13. Iodine reactor and I_2 diagnostic cell
1 – inlet tube of secondary nitrogen, *2* – secondary Cl_2 inlet tube, *3* – HI inlet tube, *4* – I_2 reactor with heating bands, *5* – I_2 diagnostic cell, *6* – optical fibre from Ar ion laser, *7* – detection Si diode, *8* – pressure reducing valve.

Technical problems concerning the data acquisition, mainly a drift in the temperature measurements was also solved during the experiments. This problem was caused by a failure of the measuring card PCI-6031E (National Instruments, USA). The data acquisition system was therefore rebuilt using a new and more versatile National Instruments CompactDAQ hardware. This new equipment consists of the NI CompactDAQ 8-slot Chassis cDAQ-9178 and four plug-and-play modules, i.e. the 16-Channel Thermocouple Input Module NI 9213, two 32-Channels ±10 V Analog Input Modules NI 9205 and 16-Channel Analog Module NI 9264.

4. Summary of results on the CentSpraySOG investigation

4.1. $O_2(^1\Delta_g)$ generation

The efficiency of the total oxygen production expressed by the chlorine utilization, U_C, is demonstrated in **Fig. 14**, showing this parameter in dependence on the total generator pressure. The chlorine utilization increased with increasing generator pressure, and decreased with increasing He content in mixture with Cl_2. This indicated that U_C increased with increasing reaction time between chlorine and BHP droplets in the spray, which was confirmed by plotting the U_C against the gas residence time in the generator, calculated by the relation

$$\tau_{gen} = V_{gen}/v_G = V_{gen}\, p_{gen}/((n_{He} + n_{Cl2})\, RT) \qquad (5)$$

where V_{gen} is the generator reaction volume (68.7 cm^3), and v_G is the total volumetric gas flow rate. This dependence is shown in **Fig. 15.**

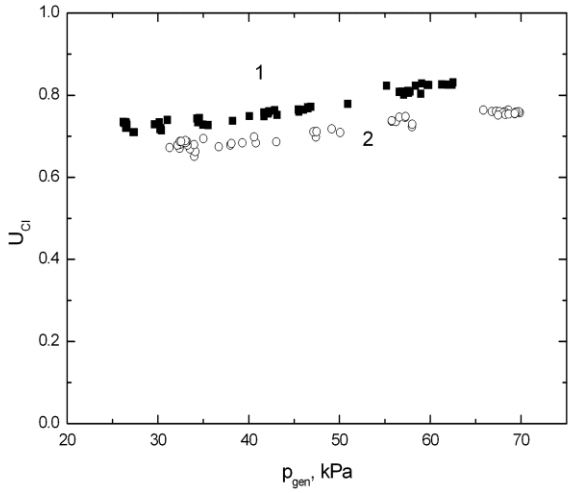

Fig. 14. Chlorine utilization in dependence on total generator pressure. Nozzle SAM-06-04, 9000 r.p.m., v_{BHP}=14 ml/s, gas flow rates (in mmol/s): 15 Cl_2 + 60 He (*curve 1*), 15 Cl_2 + 90 He (*curve2*)

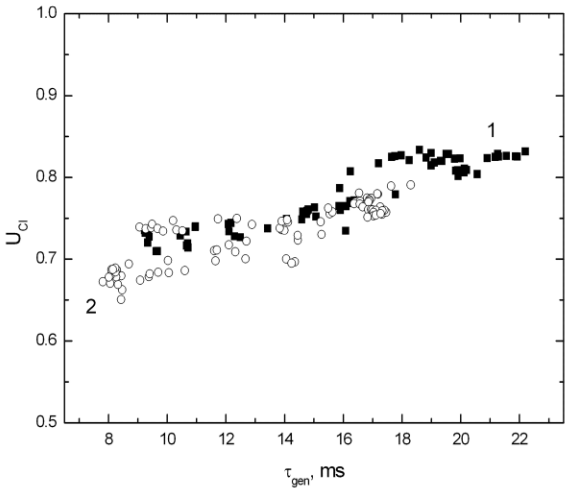

Fig. 15. Chlorine utilization in dependence on gas residence time in generator Parameters the same as in Fig. 14

Gas temperature measured in the $O_2(^1\Delta)$ detection cell located at the generator exit increased significantly with increasing gas residence time in the generator, and correlated well with the input chlorine pressure, p_{Cl2}. It can be seen in **Fig. 16**.

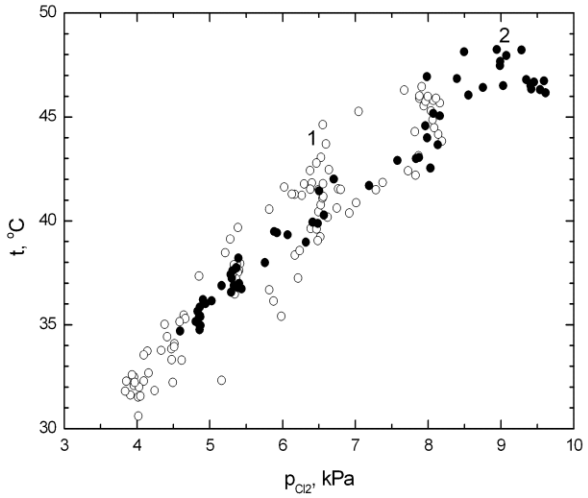

Fig. 16. Dependence of gas temperature at the generator exit on p_{Cl2} in generator.
Gas flow rates (mmol/s): 120 He + 15 Cl_2 (curve 1), 20 Cl_2 (curve 2)

The $O_2(^1\Delta_g)$ yield was significantly decreasing with the increasing input Cl_2 pressure, and this plot was independent on the Cl_2 and He flow rates, as demonstrated in **Figs. 17** and **18.**

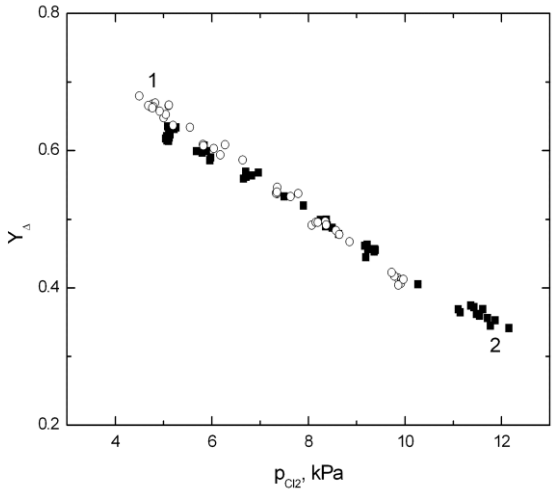

Fig. 17. $O_2(^1\Delta)$ yield in dependence on partial Cl_2 pressure.
Gas flow rates (mmol/s): 15 Cl_2 + 60 He (curve 1),
15 Cl_2 + 90 He (curve 2)

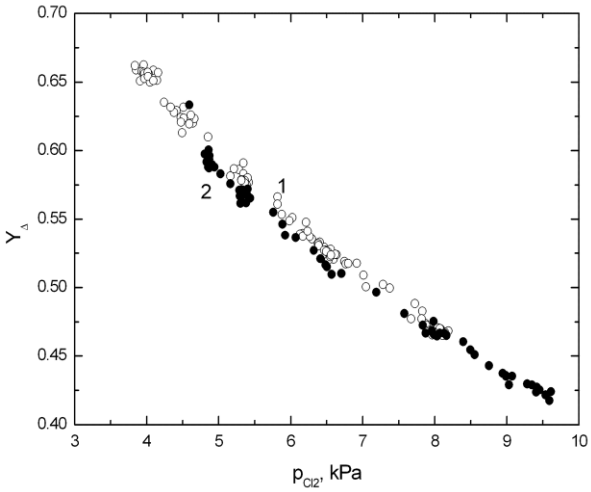

Fig. 18. $O_2(^1\Delta)$ yield in dependence on input Cl_2 pressure in the generator. Gas flow rates (mmol/s): 15 Cl_2 + 120 He (curve 1), 20 Cl_2 + 120 He (curve 2)

The rate of exothermic $O_2(^1\Delta)$ generation reaction (ΔH_1 = –123 kJ/mol) is directly proportional to p_{Cl2}, and the rates of reactions $O_2(^1\Delta)$ dimolar quenching and pooling reactions (ΔH_q = –103 kJ/mol) are directly proportional to $(p_{Cl2}U_{Cl}Y_{\Delta})^2$. This could explain why the gas temperature depended mostly on p_{Cl2} (Y_{Δ} also depends mostly on p_{Cl2}). In the generator reaction space, the temperature rise is caused by both the $O_2(^1\Delta)$ generation reaction and dimolar quenching reactions (6, 7) but this T rise is limited owing to a substantial heat capacity of liquid in the generator. It was estimated that it represents about 94% of the total heat capacity of the spray at typical gas and liquid flows in the generator (20 mmol/s Cl_2 + 100 mmol/s He + 10 ml/s BHP). The temperature increase is much faster in the gas phase due to the dimolar reactions when the BHP liquid is separated. Calculations based on the measured gas temperature in the $O_2(^1\Delta)$ detection cell and the enthalpy balance showed that the gas temperature at the reactor exit was about 20°C, and its rise to 30-50°C in the detection cell occurred during further transport time. This result was taken into account in designing the laser. The gas volume between the separator exit and pressure-reducing nozzle was therefore reduced to a minimum.

A time dependence of the $O_2(^1\Delta_g)$ yield during the transport is governed by a rate of the dimolar loss reactions of $O_2(^1\Delta_g)$ in the gas phase

$$O_2(^1\Delta) + O_2(^1\Delta) \rightarrow O_2(^1\Sigma) + O_2(^3\Sigma) \qquad k_6 = 2.7 \times 10^{-17}\ cm^3/s \qquad (6)$$

$$O_2(^1\Delta) + O_2(^1\Delta) \rightarrow O_2(^3\Sigma) + O_2(^3\Sigma) \qquad k_7 = 1.7 \times 10^{-17}\ cm^3/s \qquad (7)$$

A decrease of the yield obeys then the equation [8]

$$\frac{1}{Y} = \frac{1}{Y_o} + k_{tot}\chi \qquad (8)$$

where Y_o is the initial $O_2(^1\Delta_g)$ yield, Y is the yield measured after the transport time τ, the constant k_{tot} is given by $k_{tot}=k_6+2k_7$ = 6.1 x 10^{-17} cm^3/s. The χ parameter can be expressed as

$$\chi = \tau U_{Cl}\, c^o_{Cl2} = \tau U_{Cl}\, \frac{P_{Cl2} N_A}{RT} \qquad (9)$$

where c^o_{O2} is the initial concentration of oxygen . We estimated approximately the parameter χ using $\tau = \tau_{sep}$, where τ_{sep} was the gas residence time in the separator channels and the inlet volume of the $O_2(^1\Delta_g)$ detection cell, which was 34 cm^3 on the whole. The inverse yield $1/Y_{\Delta}$ is plotted against τ_{sep} in **Fig. 19**. Experimental constants k_{tot} = 5.7 x $10^{-17}$$cm^3$/s and 6.1 x $10^{-17}$$cm^3$/s were obtained from slopes of the lines representing the linear regression of experimental data. They agree very well with the published value k_{tot} = 6.1 x $10^{-17}$$cm^3$/s. The rate constant k_{tot} evaluated from our experiments should be significantly higher than the published value if $O_2(^1\Delta)$ is lost in the separator space also by another process, e.g. by heterogeneous quenching on the separator walls. An agreement between the theoretical and experimental value of k_{tot} also indicates that the major loss of $O_2(^1\Delta)$ takes place after leaving the

reactor space, since only separation time τ_{sep} was taken into account. The BHP flow rate affected the $O_2(^1\Delta_g)$ yield only slightly. The yield increased, e.g., from 0.48 to 0.50 when BHP flow rate was changed from 7 to 17 ml/s, which corresponded to the BHP utilization decrease from 60% to 24%. This is in a qualitative agreement with our results of modelling.

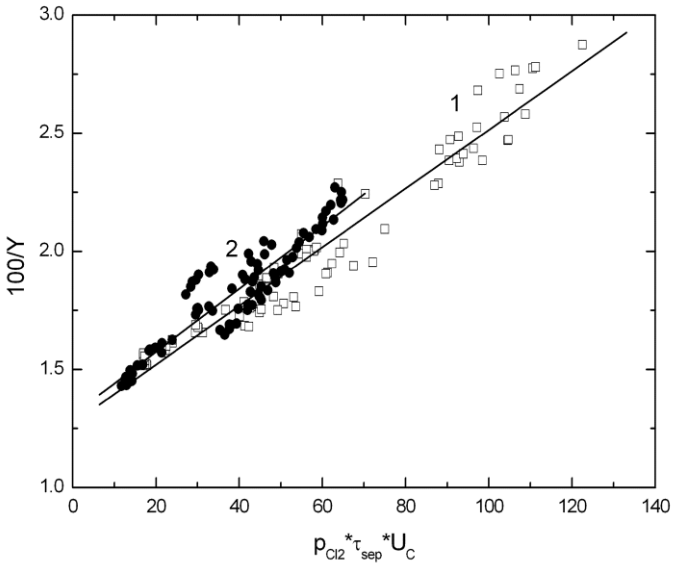

Fig. 19. Plot of $1/Y_\Delta$ vs. $U_{Cl}*\tau_{sep}*p_{Cl2}$
Gas flow rates (in mmol/s): 20 Cl_2 + 60 He (curve 1), 20 Cl_2 + 90 He (2), and 20 Cl_2 + 120 He (3); nozzle SAM-06-04, stainless steel rotor, 9000 r.p.m., v_{BHP}=14 ml/s, c_{HO2}=7.3 M

4.2. Separation efficiency of the CentSpraySOG

It was revealed that the gas dynamic pressure in the narrow slit channels of the separator had a decisive effect on droplets presence in the leaving gas. This pressure was calculated by

$$p_d = \frac{1}{2}\,\rho v^2 = \frac{n^2 MRT}{S^2}\,\frac{1}{p} \qquad (10)$$

where n is the total gas flow rate through one slit channel, M is the mean molecular weight of gas, and S is the free cross-section of one slit channel (0.8 x 50 mm^2 = 4 x 10^{-5} m^2). No droplets were detected in the gas during the whole experimental runs (up to ~5 min) with a non reactive system (9.7% NaOH solution and He-N_2 gas mixture) if the calculated dynamic pressure was ≤ 3 kPa. Some droplets appeared already within a shorter time (15-25 s) if p_d > 3.5 kPa. The effect of dynamic pressure could be ascribed to an undulating of liquid level in the slit channels that caused a detachment of new

droplets and their capturing in the gas phase. The increase in the dynamic pressure resulting in escaping of the droplets is caused mostly by either too low SOG static pressure or too high chlorine flow rate.

Results of the separation tests with the reactive BHP/Cl_2 system proved that the exiting gas was without visible droplets if the condition $p_d \leq 3$ kPa was fulfilled. This condition corresponded, e.g., to the flow of 120 mmol/s He + 20 mmol/s O_2 (formed from 20 mmol/s Cl_2) at generator static pressure ≥ 45 kPa. An example of results of measured distribution of the size of small particles by using the Spraytec instrument is shown in **Fig. 20.** It demonstrates that the liquid droplets with diameter between 0.6–2 μm are mostly present in the gas flowing from the generator. The results in this figure also proved the effect of rotation speed of the separator on the droplets concentration, which decreased substantially with increasing rotation speed from 5,000 to 9,000 r.p.m.

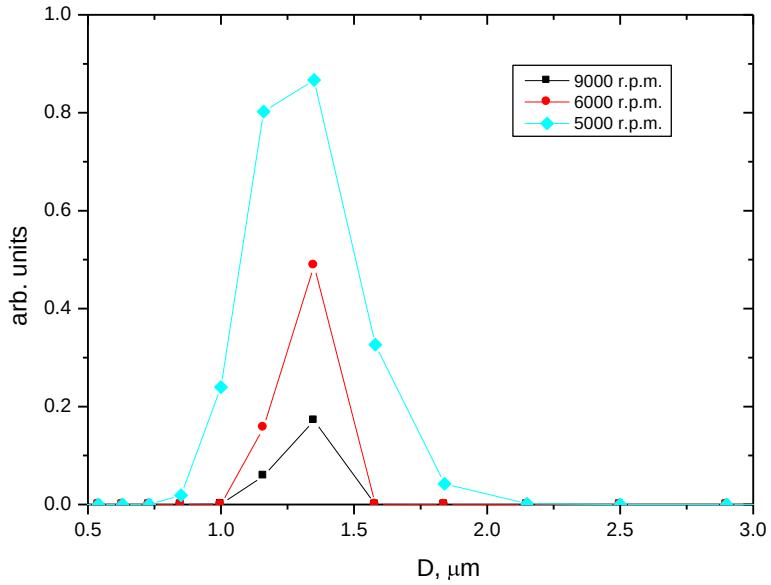

Fig. 20. Effect of separator rotation speed on droplet size distribution
Gas flow rates: 90 mmol/s He + 20 mmol/s Cl_2, P_{gen} = 50 kPa, V_{BHP} = 17.5 ml/s.

4.3. Small signal gain measurements

Many experimental sets were performed during the recent research period, aimed at measuring the small signal gain in the COIL driven by the CentSpraySOG. These experiments were performed with following input parameters of the CentSpraySOG: flow rates of 10-20 mmol/s $Cl_{2,prim}$, 60-130 mmol/s He_{prim}, a total generator pressure of 40-100 kPa, and a flow rate of BHP 15-22 ml/s. The BHP solution contained mostly 7.5 M HO_2^-. The spray nozzle SAM-06-04 was predominantly used.

For various reasons, some of these experiments were unsuccessful with regard the small signal gain; other experiments gave quite good results on this laser parameter.

4.3.1. Experiments with supersonic injection of I_2

In the first experimental series, molecular iodine was generated by the chemical method (see chap. 5), by mixing of 0.85-1.1 mmol/s HI and 0.38-0.84 mmol/s Cl_2. The I_2 yield related to Cl_2 was 0.45-0.7, which gave 0.12–0.5 mmol/s I_2. The generator (primary) gas flow consisted of 20 mmol/s Cl_2 + 90 or 120 mmol/s He, and the generator pressure was 42-50 kPa. The pressure was reduced to 5.1-6.5 kPa in the subsonic channel connecting the generator with the laser cavity, where the pressure was 1.1-1.4 kPa. In the first experiment of this series, the system was evacuated with a small-capacity pumping complex (pumping rate 0.35 m^3/s). The gas temperature measured in the subsonic channel was very high (up to 52 °C), which was also due to heating the adaptive flange (*3* in Fig. 12) by the injector body. Reducing the temperature to at most 38 °C in the next experiments was achieved by inserting a polypropylene isolating plate (10 mm thick) between the injector body and the adaptive flange. In this experimental run, no gain was detected by the iodine scan diagnostics but the absorption at 1.315 μm, and this absorption increased simultaneously with the I_2 flow rate increasing. The evaluated concentration of atomic iodine was distributed quite homogeneously across the channel, i.e. from 5 mm below the channel axis to 5 mm above the axis. The temperature in the laser cavity evaluated from ISD measurements was extremely high, 350 ± 50 K.

The second experiment was performed under similar main conditions with a difference that a more efficient pumping system was employed (the pumping rate of 0.83 m^3/s). No gain was detected again, but atomic iodine in the ground state (see **Fig. 21**). The atomic iodine concentration (more correctly $[I]-2[I]^*$) was higher at higher I_2 flow rate and increased with increasing the distance from the nozzle throat. It indicated that the dissociation efficiency increased with a distance from the throat and the dissociation rate increased with the input I_2 concentration. The concentration profile across the cavity was homogeneous at a lower I_2 flow rate, and it had a slight minimum in the cavity centre for higher I_2 flow rates. The evaluated gas temperature was also very high, 330 ± 50 K.

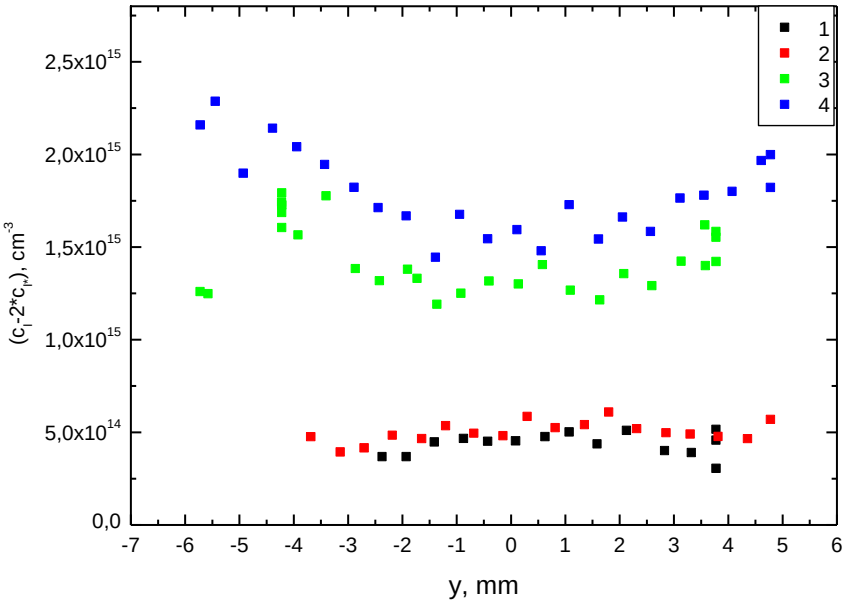

Fig. 21. Concentration profiles of atomic iodine across the cavity with chemical I_2 production
Input gas in generator: 21.5 mmol/s Cl_2 + 90 mmol/s He, p_{SOG} = 45 kPa,
input BHP flow rate: 18 ml/s (7.5 M HO_2^-), secondary gas: n_{I2} + 6.8 mmol/s N_2,
distance of ISD probe from the nozzle throat, *x*

Curve	1	2	3	4
n_{I2}, mmol/s	0.12	0.12	0.29	0.29
x, mm	47	77	47	77

In searching a reason why we did not measure the gain during these experiments, we changed the I_2 chemical source for the classical method of solid I_2 evaporation to prove if there was some detrimental effect of reagents or reaction by-products on I* and $O_2(^1\Delta)$ quenching when using the chemically produced I_2. The concentration profiles of atomic iodine measured across the cavity for the I_2 evaporation method are in **Fig. 22**. The atomic iodine concentrations and also temperature (350±50 K) are very similar for both I_2 sources.

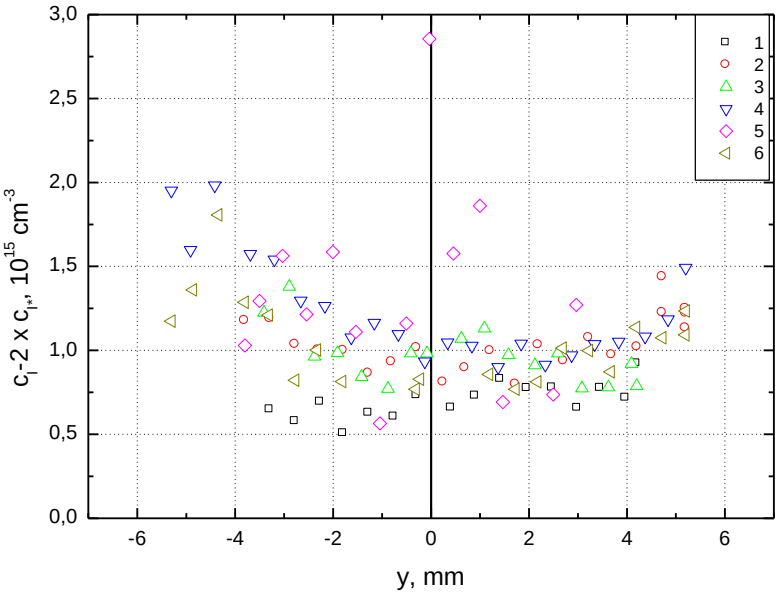

Fig. 22. Concentration profiles of atomic iodine across the cavity with evaporated solid I_2
Input gas in generator: 12 or 19 mmol/s Cl_2 + 90 mmol/s He, input BHP flow rate (7.5 M HO_2^-) 18 ml/s, secondary gas: n_{I2} + 6.7 mmol/s N_2 , distance of ISD probe from nozzle throat, *x*

Curve	1	2	3	4	5	6
n_{Cl2}, mmol/s	12.5	12.5	20.5	20.5	18.5	18.5
n_{I2}, mmol/s	0.20	0.22	0.20	0.24	0.26	0.28
p_{SOG}, kPa	37	37	46	44	45	46
x, mm	47	77	47	77	47	77

In the described experiments, some visible BHP droplets were captured by flowing gas and entrained in the laser cavity during a longer running of the generator (more than 70 s). This effect was tested also with a less concentrated BHP liquid (5.3 M HO_2^-) having a lower viscosity. For this solution, the mentioned escaping of droplets was suppressed but the BHP liquid could be cooled to –20°C only instead to –30°C. A more effective way of suppressing the droplets escaping was to reduce a diameter of the pressure-reducing orifice placed at the generator exit. It was found that the droplet escaping was sufficiently suppressed at the generator pressure of 50 kPa or higher.

In another experiments, we tested an effect of increasing I_2 flow rate from 0.05 mmol/s to 0.2 mmol/s during one experimental run. The atomic iodine concentration, c_I, evaluated from ISD measurement in the cavity centre, ($c_I - 2c_I^*$) was increased nearly directly proportional to n_{I2}. This is illustrated in **Fig. 23**. In this measurement the cavity temperature was independent on the iodine flow rate and was 310 ± 7 K. The atomic iodine concentration was estimated also from the I_2 flow rate, n_{I2}, assuming 100 % dissociation fraction and no excitation. This value was calculated by the relation

$$c_I^{teor} = \frac{2 n_{I2} N_A p}{n_{tot} RT * 10^6} \qquad (11)$$

where N_A is the Avogadro's number, n_{tot} is the total gas flow rate, and other symbols have a common meaning. The calculated atomic iodine concentrations varied from 2 x 10^{14} cm^{-3} to 6.3 x 10^{15} cm^{-3}, which quite corresponded to the concentrations measured by ISD. This result indicates that the atomic I excitation efficiency was very low.

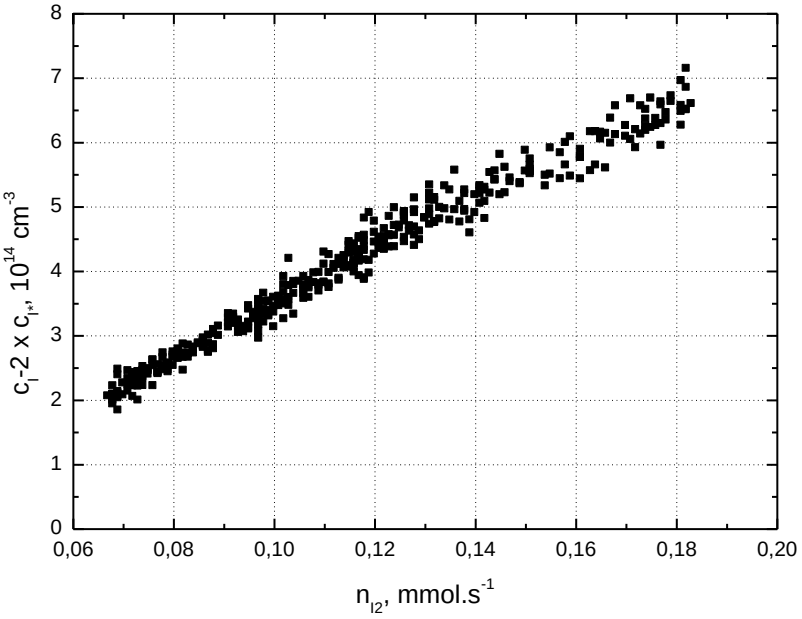

Fig. 23. Dependence of atomic iodine concentration, ($c_I - 2c_I^*$) on I_2 flow rate
Input gas in generator: 19 mmol/s Cl_2 + 90 mmol/s He, , p_{SOG} = 54 kPa,
input BHP flow rate (5.3 M HO_2^-) 20.5 ml/s,
secondary gas: n_{I2} + 11.8 mmol/s N_2, x = 54 mm

Helium was used instead of nitrogen as the secondary carrier gas in the next experiments in order to improve I_2 mixing with the primary gas flow (due to its higher diffusion coefficient). **Fig. 24** demonstrates that using helium resulted really in a more homogeneous concentration profile of atomic iodine. Also the gas temperature in the cavity evaluated from the ISD measurements was slightly lower than with nitrogen, 307 ± 15 K. This value was however much higher than a typical temperature in the COIL resonator cavity.

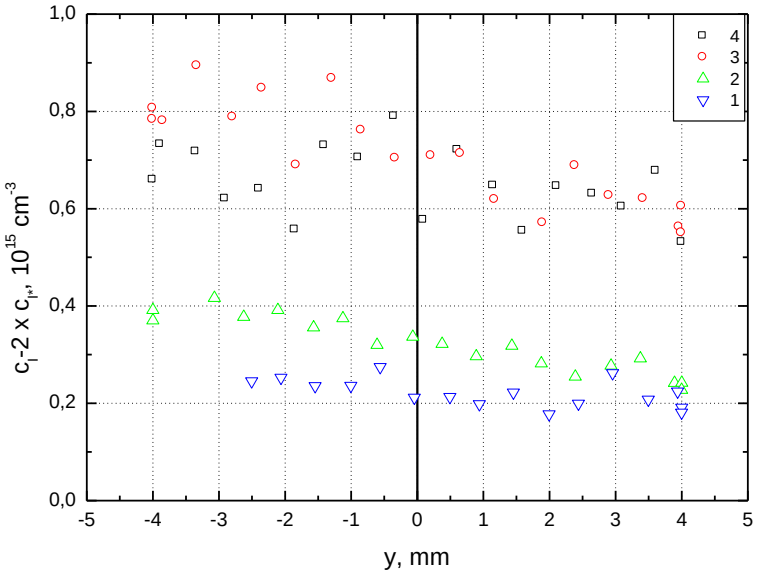

Fig. 24. Concentration distribution of atomic iodine across the cavity
Secondary carrier gas: 20 mmol/s He, BHP flow rate (with 5.3 M HO_2^-) 20 ml/s,
p_{SOG} = 49 kPa, distance from nozzle throat x = 62 mm

Curve	1	2	3	4
n_{Cl2}, mmol/s	20.5	20.5	20.5	12.5
n_{He}, mmol/s	90	90	90	60
n_{I2}, mmol/s	0.06	0.10	0.16	0.18

By this experiment we also proved coincidence between the measured data ($c_I - 2c_I^*$) and theoretical c_I calculated by the relation (11), which confirmed negligible excitation efficiency of atomic iodine.
After finishing most each of the above described experiments, we observed a tiny white deposition on inner cavity walls, originating most probably from traces of a BHP aerosol entraining with gas from the SOG. A microscopic inspection of this deposit showed that a typical diameter of these particles was about 1 μm. To avoid this phenomenon, a disc of the polypropylene felt (3 mm thick) was inserted in the exit channel from the SOG. This helped substantially to improve further experimental results.

Next experimental set was performed with n_{I2} flow in the range of 0.15-0.18 mmol/s; all other parameters were kept constant: $n_{Cl2,prim}$ = 20.2 mmol/s, $n_{He,prim}$ = 90 mmol/s, v_{BHP} = 28 ml/s, p_{SOG} = 62 kPa, $n_{He,sec}$ = 20.8 mmol/s, p_{cav} = 780 Pa. The values of ($c_I - 2c_I^*$) evaluated from the ISD measurements were (2.5 - 4.5) x 10^{13} cm^{-3}, while the theoretical values of c_I calculated from eq. (1) were by order of magnitude higher (4 - 4.8 x 10^{14} cm^{-3}). A simple calculation provided an estimate of the excited iodine concentration, c_{I*} = 1.35 x 10^{14} cm^{-3}, and the ground state iodine concentration, c_I = 3.05 x 10^{14} cm^{-3}. Only during finishing the BHP flow (lasting about 7 s) the measured ($c_I - 2c_I^*$) jumped up to 2x10^{14} cm^{-3} and then fast decreased to zero. This transient effect was probably caused by

substantial diminishing the $O_2(^1\Delta)$ concentration in primary flow at the end of experimental run, which was sufficient only for the I_2 dissociation but not yet for the I excitation to I^*. This finding convinced us that during the former experiments performed without removing very fine BHP droplets by the polypropylene felt in the SOG exit, most of the formed I^* was very efficiently quenched heterogeneously on surface of these BHP particles (droplets or crystals). Further experiments confirmed this assumption

The supersonic injection of I_2 in the primary gas flow from the SOG was shown as the unsuitable mixing arrangement. The observed no or a low population inversion of atomic iodine and very high resonator temperatures we explain (except the described effect of BHP particles) by very ineffective supersonic mixing of secondary gas with the primary gas. As a result, the diode probe diagnostics detected mostly hot jets of secondary gas with iodine, which was dissociated, but not excited to I^* effectively due to a high temperature and low $O_2(^1\Delta)$ concentration in these jets. Further experiments were therefore performed with subsonic injection of molecular iodine (see Fig. 11b).

4.3.2. Experiments with subsonic injection of I_2

All recently performed experiments with the subsonic mixing of primary and secondary flow were successful with regards the small signal gain measurement. First experiments proved that gain increased with increasing I_2 flow rate (from 0.14 to0.25 mmol/s). In next experiments the gain dependence on the distance from the nozzle throat was measured. An example is shown in **Fig. 25**.

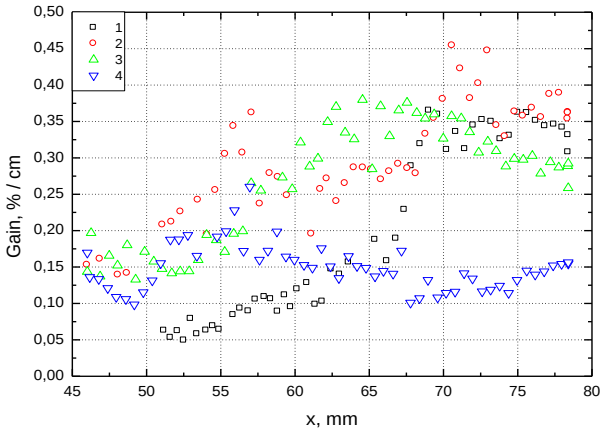

Fig. 25. Small signal gain recorded in in cavity center along the gas flow at different Cl_2 flow rates, 90 mmol/s He_{prim}, 20 ml/s BHP (with 7.5 M HO_2^-), 20 mmol/s He_{sec}, 0.3-0,33 mmol/s I_2, x – the distance from the nozzle throat

Curve	1	2	3	4
n_{Cl2}, mmol/s	8.3	11	14.4	16.5
p_{SOG}, kPa	39	43	50	54
p_{sub}, kPa	5.1	5.4	6	6.2
x_{max}, mm	73	71	65	54

The gain first increased, attained a maximum, and then decreased. The increase was obviously due to increasing extent of iodine dissociation and excitation, and following decrease by I* quenching and simultaneous decrease in the cavity pressure. A distance of the gain maximum from the nozzle was shorter for a higher $Cl_{2,prim}$ flow rate, which could be explained by increasing rate of iodine dissociation and excitation at higher $O_2(^1\Delta)$ concentration, and also by higher quenching rate. We suppose that this quenching is caused by increasing water vapour pressure since the temperature in SOG is increasing with the chlorine flow rate. Gas temperature evaluated from the ISD measurements in the cavity centre was in average 165 K, i.e., much less than with the supersonic iodine injection (310-350 K). In experiments with the subsonic I_2 injection also the gas temperature in subsonic channel was quite low, 20–25°C. Both recorded resonator temperature and gain indicated that mixing efficiency for the subsonic mixing was much better than for the supersonic iodine mixing. The gain profiles across the cavity measured in the next experimental set were parabolic with maximum in the cavity centre. It documented a good penetration of secondary gas into the primary gas.

An increasing flow rate of the primary helium shifted the position of the gain maximum still downstream from the nozzle throat (see **Fig. 26**). This can be explained by deceleration of dissociation and excitation processes caused by a higher dilution of reagents. Gas temperature in the resonator region decreased along the flow and also with increasing He flow rate. A mean temperature was between 190 K and 160 K.

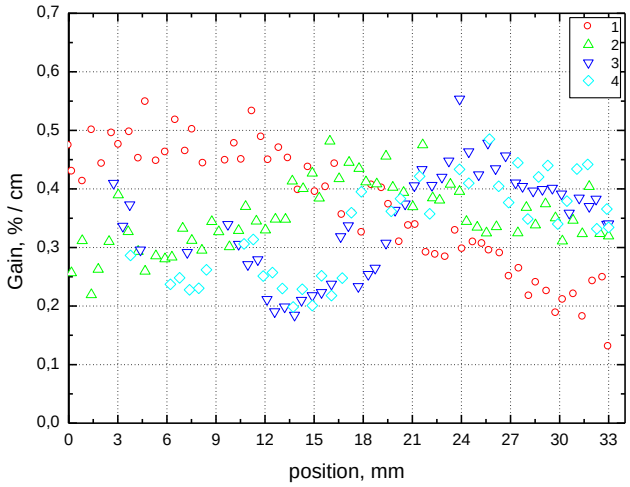

Fig. 26. Small signal gain in the cavity center recorded along the gas flow at different He_{prim} flow rates, 9 mmol/s Cl_2, 25 ml/s BHP (with 7.5 M HO_2^-), 20 mmol/s He_{sec}, n_{I2} = 0.35 mmol/s, x – the distance from the nozzle throat

Curve	1	2	3	4
n_{He}, mmol/s	70	91	110	130
p_{SOG}, kPa	36	42.5	50.5	58
p_{sub}, kPa	5.1	5.6	6.2	6.8
x_{max}, mm	53	62	70	73
p_{I2}^{subs}, Pa	18	16	15	14.5

It can be concluded from the performed small signal gain measurements that the higher values of this parameter could be obtained with the subsonic I_2 injection at higher flow rates of both chlorine and iodine. The increase in the chlorine flow rate should not increase the chlorine partial pressure resulting in significant decrease in $O_2(^1\Delta)$ yield. It would be also advantageous to increase simultaneously the BHP flow rate for high chlorine utilization and low water vapour content. This more detail investigation could not be unfortunately realized by the termination of the grant, as we lost much time by searching the reasons for the unsuccessful supersonic I_2 injection, and by a delay in fabrication of the subsonic injector.

Some of the results of investigation of the CentSpraySOG were published in Ref. [9-14].

4.4. Theoretical analysis of I* quenching in the experiment

The estimation of quenching rate has been done from the decay of small signal gain with the distance from the nozzle throat, as it was recorded in one of the experiments. The experimental data of gain and temperature together with the experimental conditions are given in **Fig. 27.**

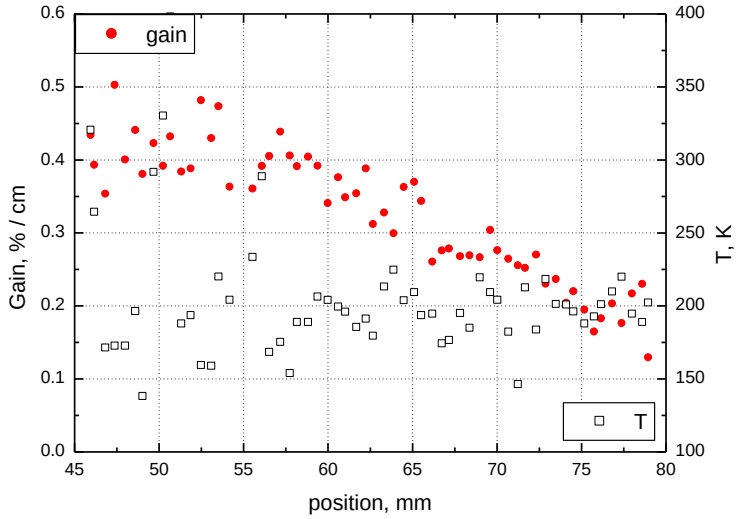

Fig. 27. Gain and temperature in the vertical center of the cavity
Flow rates (in mmol/s): He_{prim} 70, He_{sec} 20.9, Cl_2 9, I_2 0.35; cavity pressure 689 Pa, SOG pressure 36 kPa

The selected experimental case has a low chlorine flow rate, so that the loss of the $O_2(a)$ yield in I_2 dissociation will be high.

The analysis was done starting from the point of maximum gain (distance x_{max} = 52 mm) and extending to 27 mm from this point (x = 79 mm). The distance x = 46 corresponds to the leading edge of the optical window.
The formula for the small signal gain

$$g = 1.3 \times 10^{-16}/T \times 0.5[I]_{tot} \frac{(1+2K)Y-1}{(K-1)Y+1} \quad (12)$$

may be derived from the equilibrium constant of the COIL pumping reaction and the definition equation for the gain. Here Y, K and $[I]_{tot}$ are the O_2(a) yield, equilibrium constant and total iodine atoms concentration, respectively, in the diagnostic cavity. The concentration $[I]_{tot}$ is not known, but may be estimated from the formula

$$[I]_{tot} = 2\mathrm{f}\frac{\dot{\mathrm{n}}\mathrm{I}_2}{\dot{\mathrm{n}}_{\mathrm{tot}}}\frac{\mathrm{p}}{\mathrm{RT}}\mathrm{N}_\mathrm{A}\,\frac{1}{\mathrm{m}} \quad (13)$$

where f is the dissociation fraction of I_2, nI_2 its flow rate, n_{tot} the total molar flow rate, p the cavity pressure, R the gas constant, T the gas temperature, N_A the Avogadro's number and $m = [I]_{aver}/[I]_c$ is the ratio between the average concentration and the concentration in the cavity center. Because we consider only $x > x_{max}$, we assumed $f = 1$, and estimated $m = 0.8$ from the measured parabolic concentration profile. These values yield $[I]_{tot}$ = 2.18 x 10^{15} cm^{-3} at x = .65.5 mm, where the static pressure was measured.

Since the quenched excited iodine is instantaneously pumped by singlet oxygen, the loss of O_2(a) may be related to the rate of I* quenching by

$$\frac{d[O_2(a)]}{dt} = -k_q[Q][I^*] \quad (14)$$

and the loss of the yield by

$$\frac{dY}{dt} = -k_q Q_r[I^*] \quad (15)$$

where k_q is the quenching rate coefficient and $Q_r = [Q]/[O_2]$ is the ratio of the concentration of the quencher and total oxygen, respectively. These equations are valid, if the quenching is not extremely fast. The decay of Y can be obtained by integration (15) as

$$Y = Y_{max} - s(x - x_{max})$$

$$Y = Y_{max} - \frac{k_q Q_r [I^*]}{u}(x - x_{\max}) = Y_{max} - s(x - x_{max}) \qquad (16)$$

where Y_{max} is the yield at the place x_{max} of the maximum gain, u is the gas velocity, and s is the slope. Although it is not in fact true, the $[I^*]$ and the velocity u can be assumed constant, for the purpose of this simplified analysis. Knowing $[I]_{tot}$ (x) and $T(x)$, we can fit the equation (16) to the experimental gain data. The temperature was assumed to be constant along the x-coordinate, in accordance with the experimental observation. It was found that the best fit with experiment was achieved with the constant concentration $[I]_{tot}(x) = [I]_{tot,c}$ (x = 65.5 mm), Y_{max} = 0.15 and s = 1.5 x 10^{-3} m^{-1}. The decay rate (= dY/dt) is

$$r_{dec} = k_q Q_r [I^*] = s \times u \qquad (17)$$

It follows from the Pitot tube measurements that M = 1.35 and u = 840 m/s. Then, r_{dec} = 1.26 x 10^3 s^{-1}. From the equilibrium constant at T = 200 K

$$K = \frac{[I^*][O_2(x)]}{[I][O_2(a)]} = 5.51 \qquad (18)$$

the $[I^*]_c$ at x = 65.5 mm may be calculated as

$$[I^*]_c = \frac{[I]_{tot,c}}{\frac{1-Y_c}{KY_c}+1} = 9.84 \times 10^{14} cm^{-3} \qquad (19)$$

where for the Y_c it was substituted from the eq. (16) for s = 1.5 x 10^{-3} m^{-1}, Y_{max} = 0.15 and x = 65.5 mm. As it was said before, we assume for the simplicity that $[I^*](x) = [I^*]_c$. Using all the above calculated values, we can finally calculate the product k_q x Q_r = 1.28 x 10^{-12} $cm^{-3}s^{-1}$. If only H_2O was the quencher, the rate coefficient $k_{q,H2O}$ = 2 x 10^{-12} $cm^{-3}s^{-1}$ gives the ratio $Q_r = [H_2O]/[O_2]$ = 0.64. Using the partial pressure of (Cl_2+O_2) in CentSpraySOG of 3.9 kPa and 80% Cl_2 utilization, this gives the partial pressure of H_2O in the CentSpraySOG of 2 kPa, which is equal to the equilibrium vapour pressure at 290 K.

Another quencher may originate from the interaction of I^* with the residual chlorine. According to [15], ICl and Cl results from this interaction being both serious quenchers with the rate coefficients of 2 x 10^{-11} $cm^{-3}s^{-1}$ and 1.5 x 10^{-11} $cm^{-3}s^{-1}$, respectively. Because Cl is unstable, ICl could play the major role. From the value of k_q x Q_r, it yields $Q_r = [ICl]/[O_2]$ = 0.064, if the ICl was the only quencher (we neglect the H_2O presence now). Such a value would, however, require 64% of I_2 to be converted to ICl, since $2*[I_2]/[O_2]$ = 0.1. The production of the ICl and Cl is governed first of all by the relatively slow process [15]

$$I^* + Cl_2 = ICl + Cl \qquad k_{20} = 8.5 \times 10^{-14}\ cm^{-3}s^{-1} \qquad (20)$$

so we can suppose that Q_r is much less than the above estimated value and the I^* quenching by ICl is much less important than quenching by water.

Lets extrapolate Y_{max} = 0.15 upstream to the mixing point. From the analysis above, we could very roughly estimate Y_{quench} (mixing point -> window leading edge) to 0.05-0.10; from the dissociation loss, we estimated $Y_{diss} = N^*[I_2]/[O_2] = 5*0.35/9/0.8 = 0.243$ assuming that 5 O_2(a) molecules were consumed per dissociation of one I_2 molecule at 80% Cl_2 utilization. This calculation gives $Y \sim 0.5$ at the mixing point.

4.5. CFD modeling of the reactive flow between the rotor and stator

A simplified, two-dimensional CFD model was developed for the reactive flow starting from the outlet of the O_2(a) + He from the rotor slits, passing the rotor-stator inner space and escaping the stator outlet. The O_2(a) is released from two rows of holes in the rotor and during its path it is quenched by both homogeneous and heterogeneous processes. For the homogenous loss, we used the summary rate constant k_{tot} = 6.1 x 10^{-17} cm^3/s. For the heterogeneous loss, we used both the quenching probability for the stainless steel (γ_1 = 3.3 x 10^{-3}) and, because at least one wall of the rotor-stator inner space may be partially covered by BHP, we also used a more conservative estimation of γ_2= 1 x 10^{-4}. As an approximation of the situation before the gas stream reaches the slits output holes, the initial flow was split to two arms in the center of the rotor. Since the time-dependent, full 3D model would be very complicated and time-consuming for the solution, the geometry was simplified to 2D. The height of the rotor-stator inner space is changing in reality (see **Fig. 28**), the average height of 1.6 mm was used in 2D model.

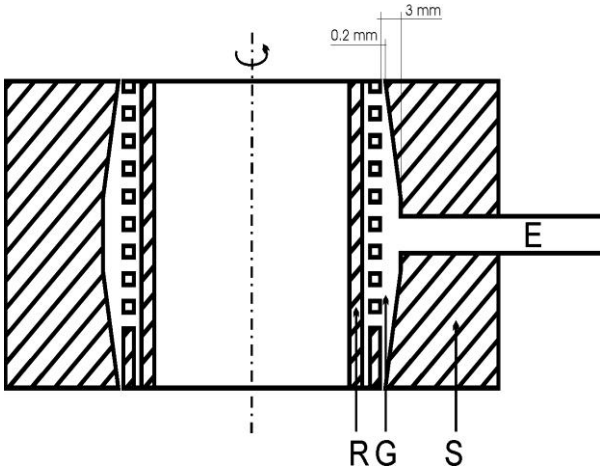

Fig. 28. Cross section of the separator rotor (R), stator (S), the gas space between them (G), and the gas exit hole (E).

Also, the cross-section of one slit outlet was set as a rectangle, having 1/9 of the total cross-section of the 9 output holes of each slit. The outer diameter of the rotor is 50 mm.
The model geometry and the computational grid are shown in **Fig.29**.

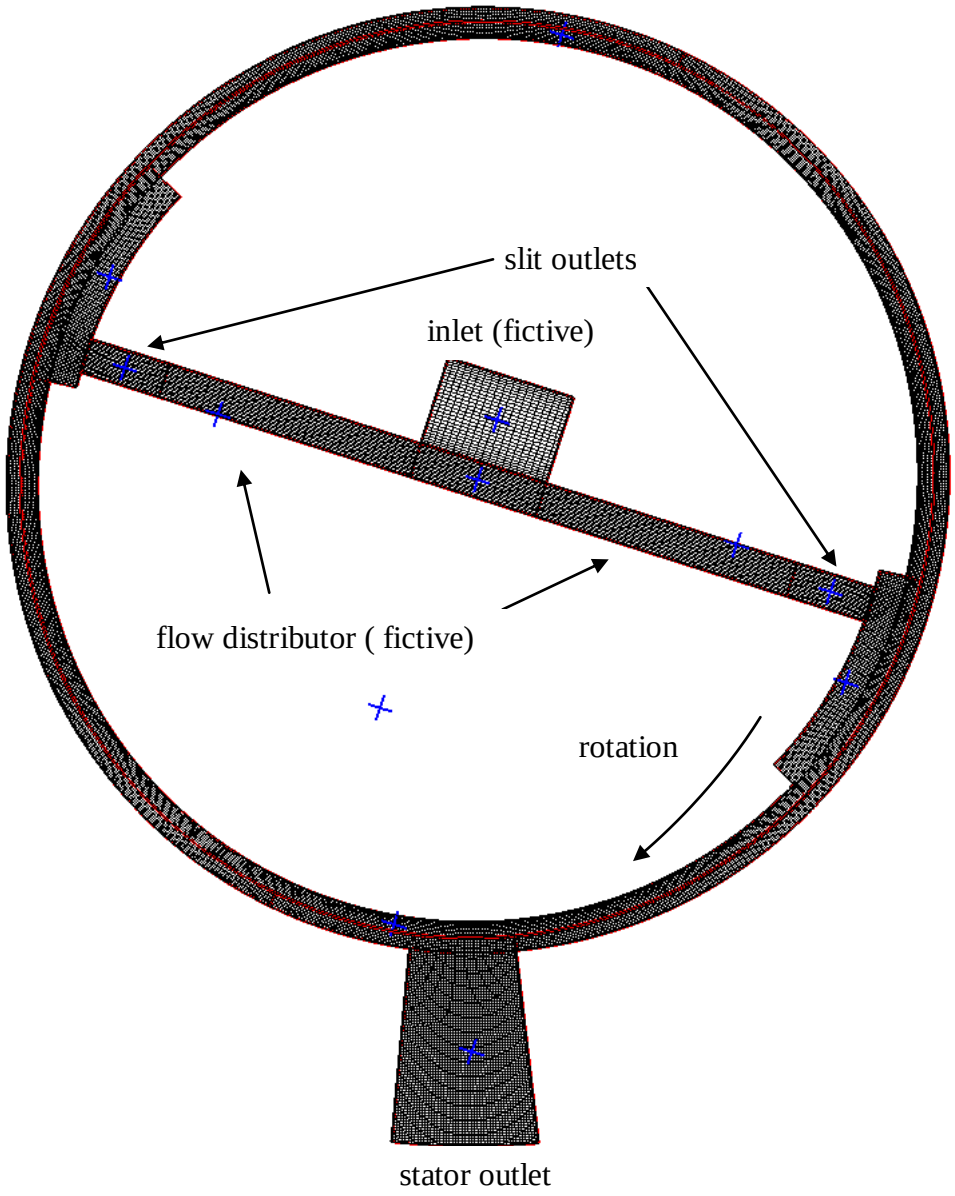

Fig. 29. Computational grid with 28152 quad cells; arbitrary interface is indicated by the red color

The model was set-up under the environment of the CFD-ACE+ multiphysics CFD software using the arbitrary moving interfaces between the grids adjacent to the rotor and stator. The grid is 3D, as it is required by the software when using the arbitrary moving interfaces option, but it uses only one computational cell in the lateral direction. In order to overcome the problems with the rotating inlets, the stator walls and the outlet were let to rotate counter-clockwise by 9000 r.p.m. In the post-

processing, the resulting velocities were recalculated relative to the "rotating" stator, so the results appear like the true moving of the rotor.

The gas pressure, flow rates and the heterogeneous $O_2(^1\Delta)$ quenching coefficient are summarized in **Table 1**. We did not intend to simulate the rotor slits volume, but the $O_2(^1\Delta)$ quenching could not be "turned off" in the fictive inner space. Instead, the $O_2(^1\Delta)$ yield was set to $Y_0 = 0.7$ at the fictive inlet, and we are only interested in the Y_1 yield at the inlet to the rotor-stator space. This value is also given in the **Table 1**. Because of different γ and O_2 flow rate these values slightly differ for the individual cases.

Tab. 1. Model conditions

Case	P, kPa	O_2, mmol/s	He, mmol/s	γ	Y_1
1	55	10	90	3.3×10^{-3}	0.53
2	55	20	90	3.3×10^{-3}	0.47
3	55	20	90	1×10^{-4}	0.53

The 100% Cl_2 utilization was assumed for simplicity.

The iterative process was started from the pre-calculated steady-state result. The velocity vectors relative to the stator in the vicinity of the stator outlet for the case 2 are shown in **Fig. 30**. This figure shows how the gas flow is affected by the rotation. The inflow to the outlet space is very asymmetric and results in a contraction of the stream to one of the outlet walls, while in the remaining space there is a counter-rotating vortex pair. This flow field is not changing during the rotation period and may be a source of additional $O_2(a)$ quenching downstream.

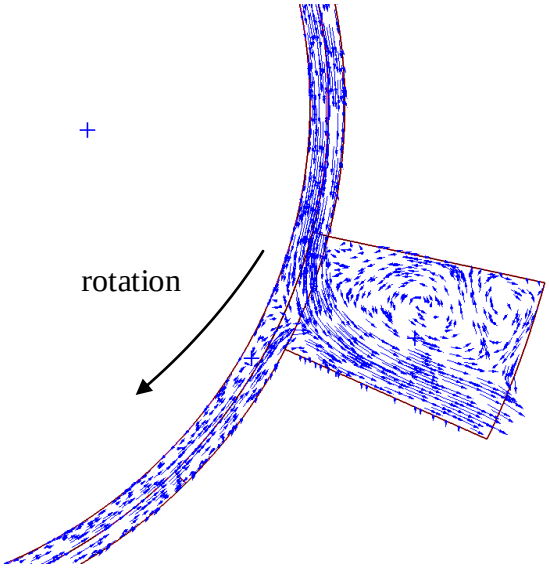

Fig. 30. Velocity vectors relative to the stator in the vicinity of the stator outlet for the case 2

The velocity vectors relative to the rotor in the vicinity of the slit outlet for the case 2, colored by the $O_2(a)$ concentration, are shown in **Fig. 31.**

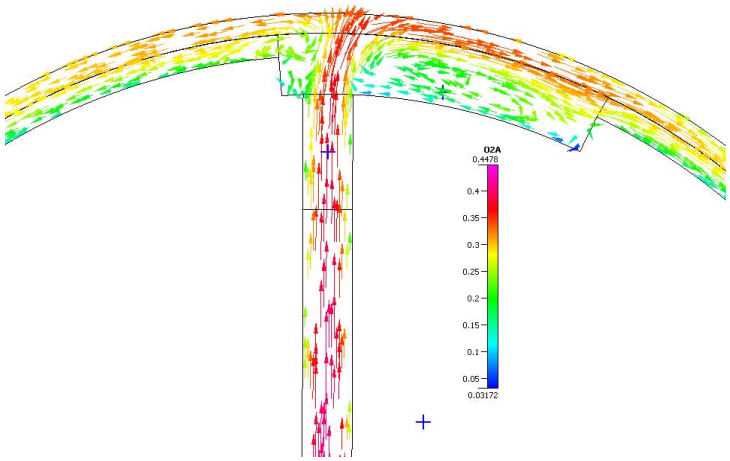

Fig. 31. Velocity vectors relative to the rotor in the vicinity of the slit outlet for the case 2
The color indicates the $O_2(a)$ concentration

Here another vortex and the $O_2(a)$ quenching are apparent on the well serving as a flow distributor among the individual holes (in the rotation-axial direction).

A time course of $O_2(a)$ yield at the stator outlet for all three cases is shown in **Fig. 32.**

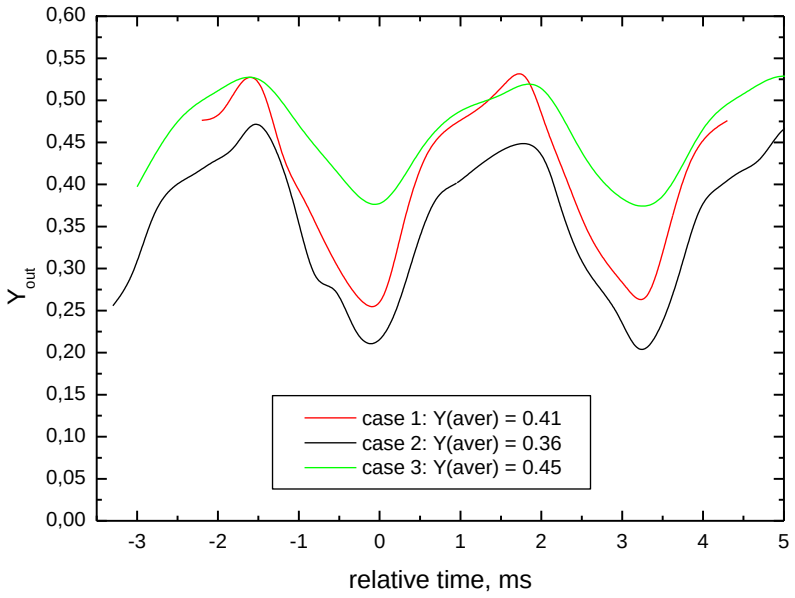

Fig. 32. Time course of $O_2(a)$ yield at the stator outlet
For the conditions of individual cases see the Table 1

A very significant variation of the outlet yield in time was obtained from the simulation. This variation is given by the varying residence time of the O_2(a) flow from the slit outlet to the stator outlet during the rotation period. The asymmetry of the curves between two minima is given by the fact that the rotation speed is added to the gas stream leaving the departing slit outlet, but it is subtracted from the gas velocity of the arriving outlet. The figure illustrates clearly that the heterogeneous loss process is more important than the homogenous one as we can expect from the very low ratio between the channel height and width (1.6/50 mm). This conclusion follows from the larger difference between the cases 2 and 3, which use a different γ value, and from the lower difference between the cases 1 and 2, which differ in the O_2 partial pressure by a factor of 2.

The partial pressure of O_2 chosen for the cases 2, 3 was 10 kPa. If we compare the calculated average yield at the stator outlet with the experimental value measured in past experiments (Fig. 16 in the interim Report 001 [18]), we can see that the result of case 3, $Y_{cav} = 0.45$ is closer to the experimental value of $Y_{exp} = 0.43$ then the result of case 2, $Y_{cav} = 0.36$. We can assess from this comparison that the rate of heterogeneous quenching can be closer to a lower value for O_2(a) quenching on the BHP wetted surface ($\gamma = 1 \times 10^{-4}$). This is supported by our experimental finding that the O_2(a) yield at the generator exit did not depend on the material of the rotor (stainless steel or Ti) although the γ_{ss} (3.3×10^{-3}) is much higher than γ_{Ti} (6.5×10^{-5}).

We plan to verify experimentally the calculated time variation of the O_2(a) yield in the CentSpraySOG.

5. Generation of molecular iodine by all-gas chemical method

In the COIL driven by the CentSpraySOG with BHP burn down system the operation time is limited to about 2-4 minutes in one experimental run. A necessary component of any I_2 evaporation system is a feedback system between the measured I_2 concentration and flow rate of carrier gas, complicating the COIL operation and decelerating needed changes in the I_2 flow rate. These reasons inspired us to propose and developed a new all-gas-phase chemical method for I_2 generation based on the reaction of hydrogen iodide and molecular chlorine [16, 17]

$$2\,HI + Cl_2 \rightarrow HCl + I_2 \qquad (21)$$

The rate constant of this reaction was not found in the literature but we estimated its value from experiments presented in the EOARD Report [18] to 1.6×10^{-16} $cm^3molec^{-1}s^{-1}$. This rate allows for a sufficient conversion of the reaction (21) in a reasonable volume, utilizing a convenient carrier gas.

5.1. Experimental configuration

Molecular iodine was produced in a reactor formed by the stainless-steel tube of inner diameter 4 cm, equipped with heating bands and optical cell for detection of the iodine concentration. A reaction

volume was 0.7 or 1.4 l. Pure Cl_2 (99.999%) and N_2 (99.9%) (Linde Gas, Ltd., CR) were used. The HI gas was synthesized in our laboratory from solid iodine, red phosphorus and water by the procedure described in Report [16]. The flow rates of all gases were measured by means of sonic orifices calibrated by the MKS mass flow meter. The gases were mixed using an ordinary T-junctions, since the diffusive mixing is thought to be sufficiently faster than the reaction rate.

The detection cell was equipped with a thermocouple, pressure transducer (Leybold, Ltd.) and Si photodiode. An output beam of Ar^+ laser at 488 nm was introduced into the cell by an optical fibre. The signal of transmitted light registered by a photodiode was fed to a photomultiplier and recorded by PC. The iodine number density $[I_2]$ was calculated using the Lambert-Beer law

$$\ln \frac{I_0}{I} = \sigma [I_2] L \qquad (22)$$

where σ = 2.47 x 10^{-18} $cm^2 molec^{-1}$ is the absorption cross-section at 488 nm [19] and L = 4.6 cm is the optical path. The intensity I at a presence of iodine was compared with the intensity I_0 immediately before starting the experiment.

Temperature of the tube reactor, and the optical cell was maintained between 90 and 130 ^oC to attain a sufficient reaction rate and to avoid iodine precipitation on the walls. The flow rate of produced iodine was calculated on-line from the measured iodine concentration, total gas flow rate, pressure and temperature using the ideal gas equation of state.

Optical detection of the laser medium was performed by the PSI Iodine Scan Diagnostics (further ISD) in the optical region from 15 to 65 mm downstream the nozzle throat. Gas temperature was calculated from the Doppler half-width on the I^*-I transition. In the experiments, the ISD probe beam was directed perpendicularly to the gas flow, in the usual direction of the COIL laser beam. The probe and the detector were moved by means of a micro-moving stage either along the gas flow (in horizontal direction) or perpendicularly to the flow (in vertical direction).

The experimental arrangement, experiments on I_2 generation and small signal gain measurements (with $O_2(a)$ delivered from the jet SOG) were described in more details in the Report 001 of this grant [20] and in publications [17, 18].

The I_2 production by this method was first studied separately, and after the process optimization, on the COIL driven by the jet SOG. The modified supersonic nozzle of the throat cross section 5 x 0.38 cm provided in a cold flow the Mach number ~2.3. The generated molecular iodine was injected in the subsonic canal through a heated iodine injector (70-90°C) with two rows of sonic orifices 0.8 and 0.4

mm i.d. in both upper and bottom wall, perpendicularly to the primary gas flow from the jet SOG. The row of larger orifices was placed 10.4 mm before the nozzle throat.

5.2. Experimental results on I_2 generation in COIL driven by the jet SOG

Few examples of experimental results on the small-signal gain and laser power are presented. Measurements of the dependence of the I_2 flow rate on the $Cl_{2,\,sec}$ flow rate at different conditions revealed that the I_2 production was saturated at the Cl_2 flow rate corresponding to a stoichiometric ratio of HI : $Cl_2 \cong 2 : 1$. The gas temperature measured in the detection cell was 90-100°C.

During the small signal gain measurements, the JSOG was operated with 20-25 mmol s^{-1} Cl_2 and 80-100 mmol s^{-1} He; the generator pressure was 8-12 kPa. The Cl_2 flow rate into the JSOG was denoted as 'primary', $Cl_{2,prim}$, and the Cl_2 flow rate into the I_2 reactor as 'secondary', $Cl_{2,sec}$. A singlet oxygen yield Y_Δ was not measured, but the extrapolation of older measurements gives an estimate $Y_\Delta \cong 0.6$. The pressure in the subsonic part of the nozzle varied between 5.2 and 5.8 kPa and the laser cavity pressure was 290-355 Pa. Considering the most common values of 5.6 kPa and 320 Pa and assuming a total pressure drop between the subsonic and supersonic part was less than 20%, the estimated Mach number was $M > 2.38$.

An example of the vertical profile of gain and temperature is shown in **Fig. 33.** The temperature falls down to 150 K at the cavity centre due to the high M. The maximum gain of 0.75 m^{-1} was obtained in these experiments, and the corresponding I_2 flow rate was 0.21 mmol s^{-1}.

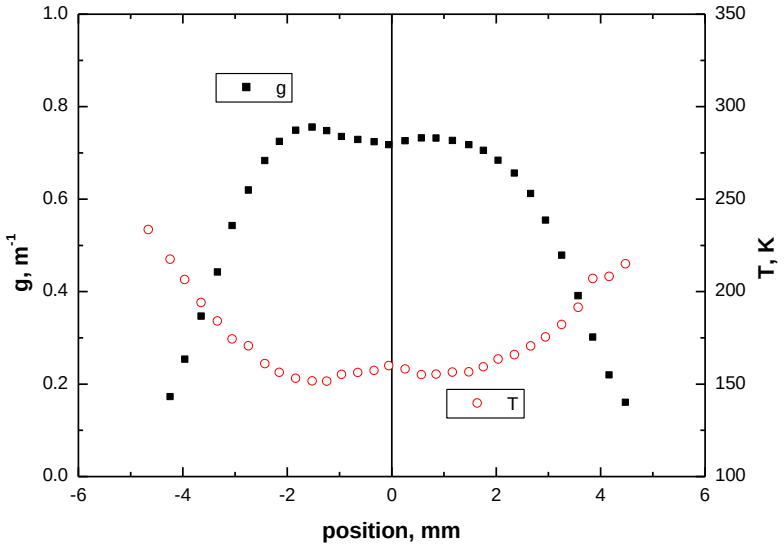

Fig. 33. Gain and temperature profile across the laser cavity
Flow rates (in mmol.s^{-1}): 20 $Cl_{2,prim}$, 85 He, 8.8 N_2, 0.5 $Cl_{2,sec}$, 0.77 HI.
Pressures (kPa): I_2 reactor 10.1, JSOG 9.6, subsonic cavity 5.6, supersonic cavity 0.318

A few laser experiments with the chemical I_2 production were then performed. Primary Cl_2 and He flow rates into the jet SOG were 19-36 mmol/s and 50-110 mmol/s, respectively. Pressure in the subsonic laser channel was typically 5.5 kPa and 350 Pa in the supersonic cavity. Mirrors of the laser resonator were of radius of curvature 5 m and 50 mm in diameter, separated by 106 cm. The active length in the flow direction (mode length) was 45 mm and the upper leading edge of the mirror was 16 mm downstream the nozzle throat. A small proportion of laser power (7.84%), separated by the glass wedge, was measured on the outcoupling mirror side. The total power was calculated as

$$P_{tot} = \frac{P_{meas}(T_1+T_2)}{0.0784T_1} \qquad (23)$$

where T_1 and T_2 are the transmissions of the outcoupling and back mirror, respectively.

Fig. 34 shows the time dependence of I_2 flow rate and laser power. Due to a relatively fast BHP temperature increase during the chlorination reaction (~6 K/min) the laser power decreased with time by about 20%. It was therefore rather difficult to measure a dependence of the power on the I_2 flow rate at constant conditions. However, the power was unexpectedly insensitive to the I_2 flow rate in the range 0.17-0.4 mmol/s and decreased significantly only when the flow rate decreased below 0.1 mmol/s. The laser power was rather insensitive to the SOG pressure. For example, a pressure change from 11.6 to 8.5 kPa increased the power from 103 to 108 W only.

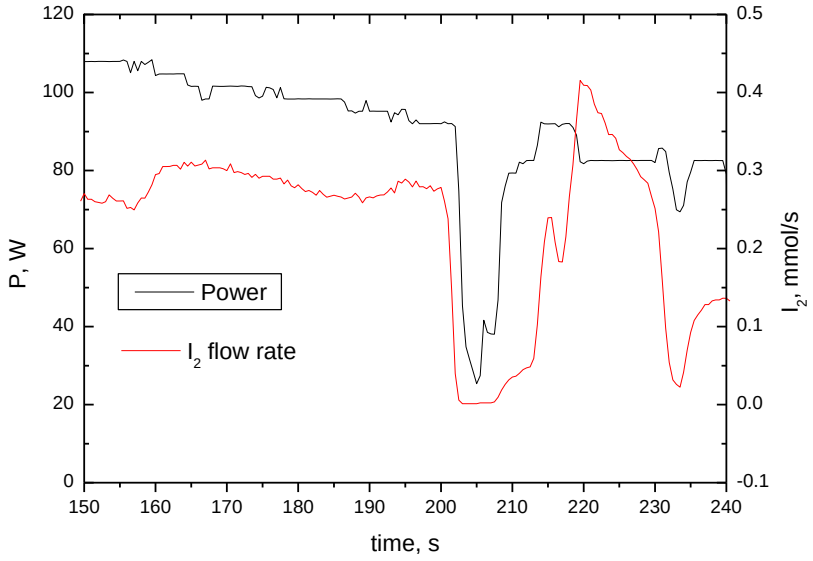

Fig. 34. Time dependence of laser output power and I_2 flow rate
Flow rates (in mmol/s): 24 Cl_{prim}, 60 He, 8.9 N_2, 0.17-0.8 Cl_{sec}, 1.34 HI; P_{gen}= 8.5 kPa;
T_1 = 1.49%, T_2 = 0.06%

A comparison of laser power generation under similar conditions with the chemically produced I_2 and classical evaporation of I_2 is shown in **Fig. 35.**

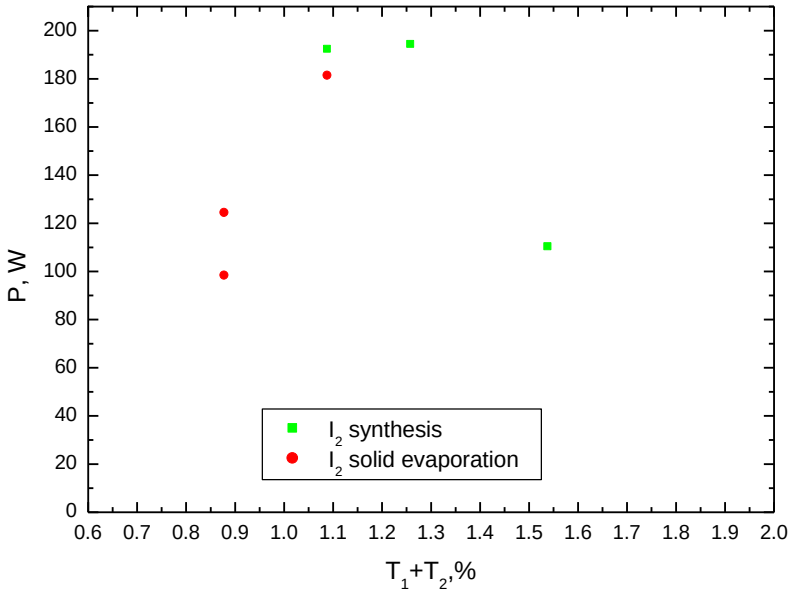

Fig. 35. Dependence of output power on the total mirror transmission
Flow rates (in mmol/s): Cl_{prim} 25, He 60, N_2 8.9-10, Cl_{sec} 0.33-0.46, HI 1.12-1.40; P_{gen}= 8.5-9.7 kPa

The same laser output power was measured with I_2 produced by both the chemical and solid iodine evaporation method. The laser power of 194 W was achieved at 22.1 mmol Cl_2/s and the total transmission of 1.27%, and was increased only to 210 W when the Cl_2 flow rate was increased to 36 mmol/s. The chemical efficiency was rather low in both cases; it did not exceed 10%. The estimated number density of I_2 was only ~5 x 10^{14} under these conditions, which was too low for efficient utilization of $O_2(^1\Delta)$ in the resonator (low extraction efficiency). It was the most probable reason of rather low chemical efficiency. The main result following from these measurements was a finding that the laser output power was practically the same with the chemical and evaporation I_2 production. The effect of reaction intermediates or products on processes in the COIL mixing region during the chemical I_2 use was not proved.

6. Conclusions

- Further modifications of the centrifugal separator construction in the CentSpraySOG device were realized, and better experimental conditions (i.e. Cl_2, He, and BHP flow rates, total pressure in the generator, the separator rotation speed, etc.) were searched to improve the separation efficiency of very small BHP droplets from generated $O_2(^1\Delta_g)$. This was achieved at 7,000 – 9,000 r.p.m. during the whole experimental runs (up to ~4 min), if the dynamic pressure in the narrow slit channels of the separator was ≤ 3 kPa, and at e.g., 20 mmol/s Cl_2 + 120 mmol/s He, and 18 ml/s BHP at the generator pressure higher than 40 kPa. In measurements with the Spraytec instrument, some droplets of the diameter 0.8 - 2 μm were detected in the exiting gas at 5000 r.p.m. Their number decreased by one order of magnitude when the rotor revolutions increased to 9000 r.p.m.
- The extensive experimental study of the CentSpraySOG operation parameters proved that $O_2(^1\Delta_g)$ is generated with a yield of 0.35 - 0.7 even at extremely high total pressures of 40 - 90 kPa (300-675 Torr), in the generator, and also at a high input Cl_2 pressure of 3 - 10.5 kPa. The $O_2(^1\Delta_g)$ yield decreased with the total generator pressure, and also with the input chlorine pressure. The yield dependence on the chlorine pressure was not affected either by helium or by chlorine flow rate. The $O_2(^1\Delta_g)$ yield in CentSpraySOG was quite comparable with the rotating disc, jet, and aerosol generators, but it was attained at significantly higher generator pressures, and mostly for higher input chlorine pressures. The chlorine utilization, U_C, increased with increasing reaction time in the generator, and was not affected by changing the BHP flow rate when the BHP utilization varies from 0.24 to 0.6. The U_C values (~0.7 - 0.88) were comparable with data typical for the aerosol and twisted aerosol generators. They are obviously lower than in rotating disc and jet generators but they can be achieved at much higher generator pressures. A very high BHP utilization (up to 80%) at the single pass burn down CentSpraySOG operation is exceptional in comparison with other generator types; this would be beneficial for reducing the weight of the whole laser system in the mobile COIL applications thanks to less consumption of the BHP liquid for its operation.
- A relative high temperature (30–50°C) measured in the $O_2(^1\Delta_g)$ detection cell was explained by the $O_2(^1\Delta_g)$ quenching mostly during the gas transport after the liquid separation. This was verified by experiments with the COIL driven by the CentSpraySOG, in which a volume of the gas channel downstream the separator was minimized resulting in a gas temperature decrease in the subsonic channel to 20–25°C.
- Designing and manufacturing of individual components of the COIL device joined to the CentSpraySOG, and furnishing the device with necessary diagnostic instruments and data acquisition system involving elaboration of special software took up much time.

- The new method for molecular iodine generation by all-gas chemical procedure was developed and employed in the laser experiments, first examined on the COIL driven by the jet SOG, and then by the CentSpraySOG. It was experimentally proved that both the small signal gain and laser output power were practically the same at employing this chemical method and usual I_2 evaporation. The results showed that the reactants, intermediates, or reaction products of the chemical method did not significantly quenched $O_2(^1\Delta_g)$ and I^*. Molecular iodine produced by this method can be fast and easily controlled by the HI or Cl_2 flow rates; it should be also easily scaled-up.
- The small signal gain measurements on the COIL driven by the CentSpraySOG were performed with the supersonic and subsonic I_2 injection. In the many experimental sets with the supersonic injection, no positive gain was recorded at different conditions. Atomic iodine in the ground state was mostly detected, and very high temperature (310–350 K) was measured. This result was explained by bad mixing of the secondary I_2 gas with the primary $O_2(^1\Delta_g)$ flow. In the COIL measurements with the subsonic I_2 injection, positive gain was measured at low temperatures (160–200 K). The parabolic gain profile across the channel proved a proper mixing of primary and secondary flows. The ssg values were up to 0,5 %/cm, but the conditions were not optimized yet by termination of the grant. An increase in the I_2 and Cl_2 flow rates will be profitable.
- Comparison of the measured gain dependence on distance along the flow with the mathematical model showed that water vapour is much more efficient quencher than ICl in our COIL system with the CentSpraySOG. The modeling of the gas flow in separator channels indicated some 'weak points' of the separator design, where some $O_2(^1\Delta_g)$ can be lost. Modifications of the separator design are therefore planned.

Plans for the next work:

- After accomplishing the ssg measurements with the subsonic I_2 injection, experiments with lasing on the COIL with the CentSpraySOG will performed, i.e. the task D in the grant proposal (see p. 4) will be fulfilled.
- Some modification of the COIL device will be designed and manufactured to test it at higher pressures and so to benefit from the high-pressure operation of the CentSpraySOG.

References

[1] Final Report of the USAF EOARD, Grant No. FA8655-05-C-4022, submitted 28 Feb 2007 (J.Kodymová)

[2] Final Report of the USAF EOARD, Grant No. FA8655-05-C-4022, submitted 30 Apr 2008 (J.Kodymová)

[3] J. Hrubý, O. Špalek, V. Jirásek, M. Čenský, J. Kodymová, *Development of new chemical generator of singlet oxygen: Centrifugal separator of gas and liquid phases*, COIL R&D Workshop, Stuttgart 2005. CD Proceedings

[4] J. Kodymová, O. Špalek, V. Jirásek, M. Čenský, J. Hrubý, *Development of advanced generator of singlet oxygen for a COIL*, High Power Laser Ablation Conference, Taos, NM, USA, May 2006, Proc. SPIE 6261, 62611S1-S11, 2006

[5] O. Špalek, J. Hrubý, V. Jirásek, M. Čenský, J. Kodymová, I. Picková, *Advanced spray generator of singlet oxygen,* XVI Inter. Symposium on Gas Flow and Chemical Lasers, and High Power Laser, GCL/HPL 2006, Gmunden, Austria, Sept 2006, Proc. SPIE Vol. 6346, 63460C1-C9, 2006

[6] J. Kodymová, O. Špalek, V. Jirásek, M. Čenský, I. Picková, *A centrifugal spray singlet oxygen generator for a chemical oxygen-iodine laser,* 38th AIAA Plasmadynamics and Lasers Conference, Miami, FL, USA, June 2007, AIAA Paper 2007-4622, CD Proceedings

[7] O. Špalek, V. Jirásek, M. Čenský, J. Kodymová, I. Picková, *Spray generator of singlet oxygen with a centrifugal separation of liquid,* 17th Int. Sym. GCL-HPL, Lisbon, Portugal, Proc. SPIE Vol. 7131, 7131OH1-9, 2008

[8] T. L. Rittenhouse, S. P. Phipps, and Ch. A. Helms, IEEE J. Quantum Electron. 35, 857 (1999)

[9] J. Kodymová, V. Jirásek, J. Schmiedberger, O. Špalek, M. Čenský, *Research on advanced chemical and discharge oxygen-iodine lasers*, Proc. SPIE Vol. 7196, 719602-1-11, 2009

[10] O. Špalek, V. Jirásek, M. Čenský, J. Kodymová, Jan Hrubý, *Centrifugal spray $O_2(^1\Delta_g)$ generator,* COIL R&D Workshop, Stuttgart, Oct. 2009

[11] J. Kodymová, V. Jirásek, J. Schmiedberger, O. Špalek, M. Čenský, *Research on advanced chemical and discharge oxygen-iodine lasers*, Optics and Spectroscopy 107, 876-885, 2009

[12] V. Jirásek, J. Hrubý, O. Špalek, M. Čenský, J. Kodymová, *Spray generator of singlet oxygen for a chemical oxygen-iodine laser*, Appl. Phys. B, 2010, DOI: 10.1007/s00340-010-4060-4

[13] O. Špalek, J. Hrubý, M. Čenský, V. Jirásek, J. Kodymová, *Centrifugal spray generator of singlet oxygen for a chemical oxygen-iodine laser*, Appl. Phys. B, 2010, DOI: 10.1007/s00340-010-4061-3

[14] J. Hrubý, O. Špalek, J. Kodymová, V. Jirásek, M. Čenský, *Způsob generace kyslíku v singletovém delta stavu a generátor pro provádění tohoto způsobu*, CR Patent 301 755, 2010 (in Czech)

[15] A.V. Komissarov, M.C. Heaven, *J. Phys. Chem.* 107 (49), 10527-10532, 2003

[16] Report 001 of the USAF EOARD, Grant No. F61775-00-WE032, submitted 24 July 2000 (J. Kodymová)

[17] V. Jirásek, M. Čenský, O. Špalek, J. Kodymová, *Chemical Generation of Molecular Iodine for a COIL*, US AF EOARD COIL R&D Workshop, 13-14 Oct, 2009, Stuttgart, Germany, CD Proceedings

[18] V. Jirásek, O. Špalek, M. Čenský, J. Kodymová, *Measurement of small-signal gain on COIL with chemically generated molecular iodine*, IEEE J. Quant. Electron., 2010, DOII 10.1109/JQE.2010.2048555

[19] R.W. Saiz-Lopez, D.M. Saunders, Joseph S.H. Ashworth, J.M.C. Plane, *Absolute absorption cross-section and photolysis rate of I_2*, Atmos. Chem. Phys. Discuss. 4, 2379-2403, 2004

[20] Report 001 of the USAF EOARD, Grant No. FA8655-09-1-3091, submitted 22 Nov 2009 (J. Kodymová)

[21] Report 002 of the USAF EOARD, Grant No. FA8655-09-1-3091, submitted 22 Mar 2009 (J. Kodymová)

Acknowledgements

The investigators are very grateful to the US AFRL/DED at Kirtland AFB, NM for the financial support of this research via the USAF EOARD grant.

We wish to thank Dr. Timothy Madden at the AFRL/DED for beneficial discussions on the contract tasks and supporting our research.

We also thank Dr. Tom Gavrielides, Program Managers Laser and Electro-Optics, Mrs. Susan Fuller, Contracting Officer, and Mrs. Jeannette Cyrus, Program Analyst, at the USAF EAORD for their very valuable assistance with the Grant processing.